4D THERMAL AND PETROLEUM SYSTEMS MODELLING OF THE CENTRAL SCOTIAN SLOPE IN AND AROUND THE EASTERN SHELBURNE SUB-BASIN

Eric W. Negulic

Submitted in Partial Fulfillment of the Requirements
for the Degree of Bachelor of Science, Honours
Department of Earth Sciences
Dalhousie University, Halifax, Nova Scotia
April 2008

DALHOUSIE UNIVERSITY
Inspiring Minds

Department of Earth Sciences
Halifax, Nova Scotia
Canada B3H 4J1
(902) 494-2358
FAX (902) 494-6889

DATE: April 21st, 2008

AUTHOR: Eric W. Negulic

TITLE: 4D Thermal and Petroleum Systems Modelling of the Central Scotian Slope in and Around the Eastern Shelburne Sub-basin

Degree: BSc. Convocation: May 2008 Year: 2008

Abstract

Early hydrocarbon discoveries in the Sable sub-basin on the Scotian Margin have resulted in the primary exploration focus on the Sable and adjacent Abenaki sub-basins with lesser focus on the surrounding sub-basins and seaward slope, despite the presence of thick regional sedimentary cover. This thesis aims to broaden our knowledge of the slope area immediately southwest of the Sable sub-basin, with emphasis on heat-flow and petroleum systems potential. The Scotian slope is highly deformed by the thick Argo salt that forms many salt structures such as salt diapirs, tongues and canopies. Salt has a high thermal conductivity and the presence of diapirs results in significant variations in heat-flow throughout the Scotian Slope affecting hydrocarbon maturation. A 4D model was created to study the thermal and petroleum systems properties of the region in and around the eastern Shelburne sub-basin. The model is constrained by seismic interpretations of four lines bounding the study area, well data and analogue models. The goal of the model is two fold: 1) predict the effect of salt diapirs on heat-flow, and 2) predict the petroleum systems potential under idealised conditions. The model shows significant increases in heat-flow in regions overlying salt diapirs, as well as the accumulation of hydrocarbons in selected reservoirs. The predicted heat-flow values are used to suggest locations for heat-flow measurements to be taken in the summer of 2008, and these measured values will then be used to calibrate future models of the area.

Key Words: Heat-flow, Scotian Slope, 4D modelling, petroleum systems, salt tectonics.

Table of Contents

List of Figures

List of Tables

Acknowledgments

First and foremost I would like to thank Dr. Mladen Nedimovic and Dr. Hans Wielens for providing me with the opportunity to work on this great project and for their supervision. If it weren't for their expertise, assistance and great patience this project would not have been possible. I would like to extend a special thank you to Dr. Keith Louden and Dr. Juergen Adam for their continued assistance and expertise throughout the course of this project. I'd also like to thank all my professors at Dalhousie for their encouragement and help both on this project and throughout my undergraduate degree. Thank you to GX Technologies for the use of their NovaSPAN lines, Integrated Exploration Systems (IES) for allowing me the use of their wonderful PetroMod 10 software, and Shell Canada for their funding and support that got this project started. I want to acknowledge all my classmates for being great friends and for making school a fun place to be. Finally I have to thank my parents for all their support and for making this possible.

Chapter One: Introduction

1.1 Project motivation

The Scotian Basin has been the site of extensive hydrocarbon exploration throughout the late 20th century and continues on to be into the 21st century. Exploration has been focused primarily on the Abenaki and Sable sub-basins in the eastern portion of the Scotian Basin, with less extensive exploration in more western regions such as the Shelburne sub-basin, despite its thick sedimentary fill. Currently, the only production in the Scotian Basin is from the Sable Gas Project, which has produced upwards of 12.5 million m^3 of natural gas per day, and is expected to continue its production into the 2020's (Enachescu and Hogg, 2005). Despite this past success, the latest phase of hydrocarbon exploration has been largely unsuccessful in locating potential source and reservoir rocks in recent wells drilled in the shallow water shelf regions and along the deep-water continental slope (Enachescu and Wach, 2005). The lack of recent success suggests that there is a need for a better understanding of the Scotian margin's complex geology, particularly in the shelf-slope-basin transition, if better constraints are to be placed on where future hydrocarbon exploration may be more successful.

1.2 OETRA project

To broaden our understanding of the Scotian Basin and therefore stimulate petroleum exploration in the area the Government of Nova Scotia has formed a new agency called the Offshore Energy Technical Research Association (OETRA). Louden and Nedimovic of Dalhousie University in collaboration with Mukhopadhyay at Global Geoenenergy Research Limited have a three year project entitled "Analysis of petroleum systems on the Scotian slope using thermal and seismic techniques" funded by a grant

from this agency. I will refer to this project as the OETRA project. The research done for this honours project is tied to the OETRA project. The OETRA project focuses on thermal and petroleum systems modelling, and will include analysis of petroleum potential and heat-flow analysis in regions of autochthonous salt diapirs and allochthonous salt canopies. The project will also include analysis of seismic reflection data from GX technologies NovaSPAN survey of the Scotian Basin. Heat-flow and seismic interpretations will be done at Dalhousie University, while petroleum systems modelling will be done at Global Geoenergy Research.

The project is divided into two phases, focusing on different regions of the Scotian Slope and deepwater regions of the Scotian Basin. Phase one focus is on the eastern portion of the Shelburne sub-basin and surrounding areas located in slope diapiric subprovince II (Shimeld, 2004) (Fig. 1.1). Phase two focuses on the Sable sub-basin and surrounding regions contained in slope diapiric subprovince III (Shimeld, 2004) (Fig. 1.1). The goal is to compare heat-flow measurements in the two regions and their variations over salt structures, and to tie the resulting variations to petroleum systems maturation potential between the regions. Seismic data will be used to characterize the physical properties of the sediments for defining possible reservoir sands based on high definition velocity models (Keith Louden, personal communication. 2007). The thermal and petroleum systems modelling portion of this honours project fits in with the phase one region of the OETRA Project, and will be used for comparison with the modelling done at Global Geoenergy Research Limited in order to help constrain regions for heat-flow measurements to be collected in the summer of 2008.

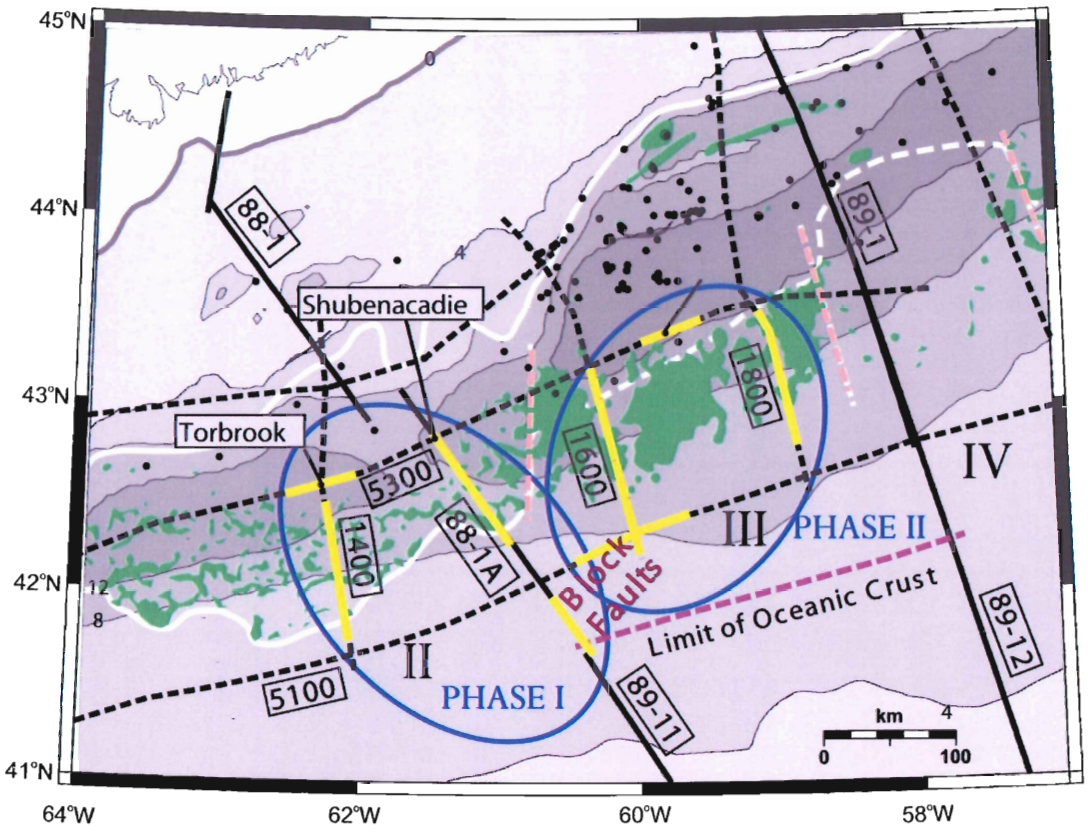

***Figure 1.1**: Map of Scotian margin with slope diapiric subprovinces and OETRA phase locations. Green represents salt, slope diapiric subprovinces II, III, and IV are separated by dashed pink lines, yellow lines represent regions of seismic lines to be interpreted for the OETRA project, white lines outline initial salt basin locations and black dots represent wells (from Nedimovic personal Dalhousie webpage; http://myweb.dal.ca/ml234413/) .*

1.3 Objectives

The goal of this project is to develop and further our understanding of the heat-flow and petroleum systems potential of the Scotian Slope within and surrounding the eastern regions of the Shelburne sub-basin. To do this I produced a 4D thermal and petroleum systems model for the region using PetroMod 10 software. In order to create an accurate model, all available information derived from seismic images, well data, and analogue models from the region was used.

Analogue modelling experiment 5-7 was created and interpreted in order to gain insight into the evolution of salt deformation structures within the Scotian Basin. The model contained an initial symmetrical full graben basement structure with thick salt fill, followed by seaward prograding sedimentation atop the salt, a common yet simplified feature in rift related passive margins. The model has been interpreted and structurally restored to provide insight into the evolution of the salt structures in the Scotian Basin.

Four intersecting seismic lines, GXT NovaSPAN lines 1400, 5100, and 5300, and Lithoprobe line 88-1a, form the perimeter of the study area for thermal and petroleum systems modelling. These seismic profiles were interpreted with Kingdom Suite software, depicting specific age boundaries and formation tops, as well as salt deformation, and basement structures. Information gathered on the evolution of salt diapirs in the analogue models is used to constrain diapir evolution in the 4D thermal and petroleum systems model.

The thermal and petroleum systems model will be used to help constrain regions for future heat-flow measurements to be taken in the summer of 2008 as part of the OETRA project. The heat-flow predictions from the model created in this project will be compared with those from Global Geoenergy Research Limited to provide a second possible heat-flow interpretation of the region. The goal of creating this 4D model was not only to provide an interpretation of the possible petroleum systems and heat-flow within the study area, but also to provide suggestions for future work to be done in order to further our understanding of this complex region.

1.4 Geologic setting

The Scotian Basin runs approximately 1200 km from the Yarmouth Arch just southwest of the Canada/U.S. border, to the Avalon uplift of the south-western Grand Banks of Newfoundland and with an average width of 250 km covers an area of approximately 300,000 km^2 (Kidston et al., 2002). The Scotian Basin formed as a passive continental margin during the rifting of Pangaea as the African plate separated from the North American plate in the Late Triassic to Early Jurassic (Wade et. al., 1995). A series of basement grabens and half-grabens formed in the Scotian Basin during rifting including the Shelburne, Sable, Abenaki, Laurentian, and South Whale sub-basins, and the Orpheus Graben (Fig. 1.2). Other basement lows include the Naskapi Graben complex and the Mohican Graben (Shimeld, 2004).

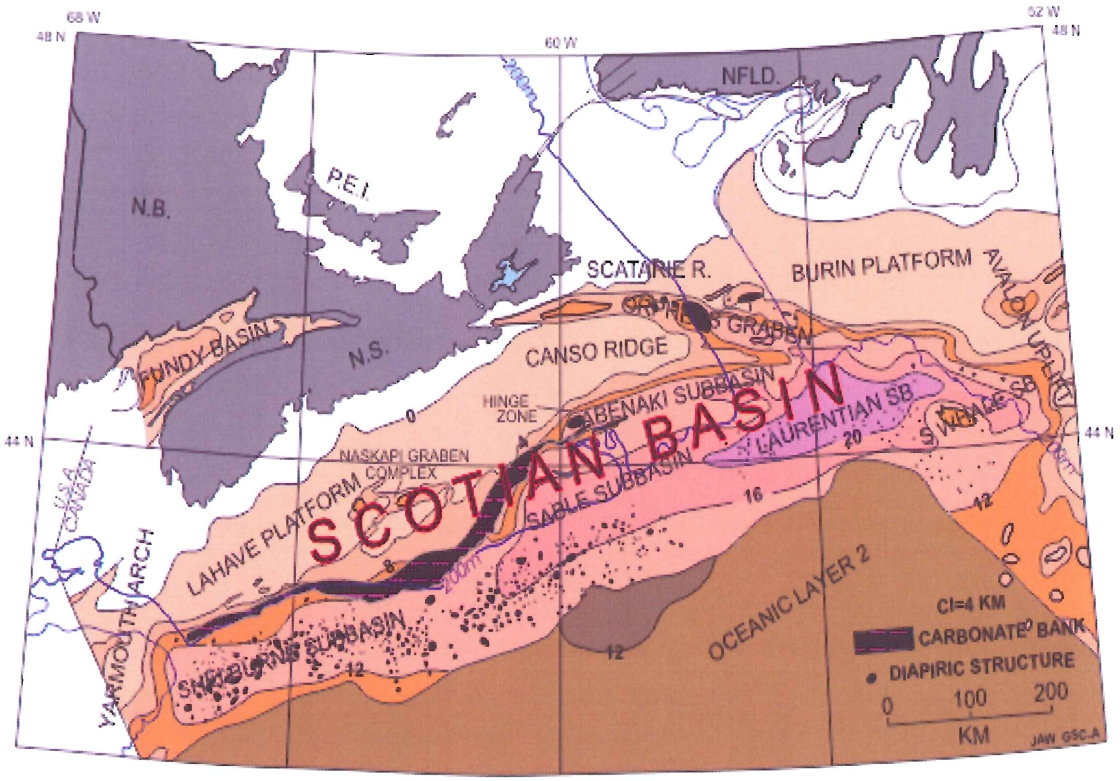

***Figure 1.2**: Map of the Scotian Basin including all major sub-basins. Background map is sediment thickness (from http://gsc.nrcan.gc.ca).*

1.4.1 Rifting and formation of the Scotian Basin

During the Late Paleozoic, eastern North America was connected to northern Africa in the central regions of the supercontinent Pangaea. The region that today makes up the east coast of Nova Scotia was located at the paleo-equator and experienced a hot, dry climate during the Triassic (Jansa and Wade, 1975). The current-day Scotian Basin was formed as a result of rifting of the supercontinent Pangaea in the Late Triassic, followed by continental drift which moved North America to its present location (Jansa and Wade, 1975).

Rifting began in the Late Triassic and resulted in initial thinning of the crust and extensional block faulting forming a series of basement lows as grabens and half grabens which formed depocenters for thick sediment packages (Hyndman et al., 1975). Further post-rift basin subsidence resulted from thermal contraction as well as sediment loading of the crust (Hyndman et al., 1975). As the Pangaean continental plate thinned during extension, mantle upwelling and intrusion into the thinned crust caused temperature increase accompanied by thermal expansion and uplift of the crust. The uplifted regions return to their original height by thermal contraction over a period of ~50 Ma (Hyndman et al., 1975). A second major cause of crustal subsidence was sedimentary loading in the basins. This subsidence occurs because as sediment is deposited, it replaces a volume previously consumed by less dense sea water, and to compensate for the density change the crust lowers (Hyndman et al., 1975).

1.4.2 Lithologies and stratigraphy of the Scotian Basin

The generalized stratigraphy of the Scotian Basin is shown in Figure 1.3. It should be noted that many of the lithologies present in the Scotian Basin tend to shale out as they

extend basinward down the continental slope. Constraints from wells in the deepwater are limited, and thus interpretation of formations and lithologies in these regions is difficult. The following summary of the stratigraphy of the Scotian Basin is based on the work done by Jansa and Wade (1975), Wade and MacLean (1990), and Kidston et al. (2002).

The oldest stratigraphic units are syn-rift redbeds of Late Triassic age. These redbeds were deposited during the initial rifting of Pangaea under arid conditions in a fluvial/lacustrine environment. The next unit consists of the red clastic carbonate sediments of the Eurydice Formation, deposited in restricted shallow marine environments during the Late Triassic to Early Jurassic. This unit consists of ~45% shale, 45% thin siltstone and sandstone layers, and the remaining portions are minor evaporites and limestones. Following the onset of deposition of the Eurydice came the thick salt deposits (~2 km) of the Argo Formation which interfinger the Eurydice Formation. This unit was deposited at elevations below sea level in a hot and arid climate with abundant evaporation resulting in the formation of the thick salt layers. This evaporite unit is of Early Jurassic age and contains relatively pure salt with a very low anhydrite content.

The renewed tectonic activity in the Early Jurassic that caused faulting of these previously described sedimentary units is referred to as the break-up unconformity. Following the break-up unconformity and unconformably overlying the Argo salt are the thick dolomite deposits of the Iroquois Formation. This unit was deposited in a shallow water to inter-tidal environment during the Sinemurian to Pliensbachian. The Iroquois Formation was deposited as a result of a transgressive pulse as the rift basin became inundated. The clastics of the Mohican Formation are composed of dolomitic siltstones

and fine grained sandstones, interbedded with shales, and overlie the Iroquois Formation. This unit levelled off the remaining basement fault block basins and covers the remaining basement highs. Deposition occurred in a Bajocian fluvial environment.

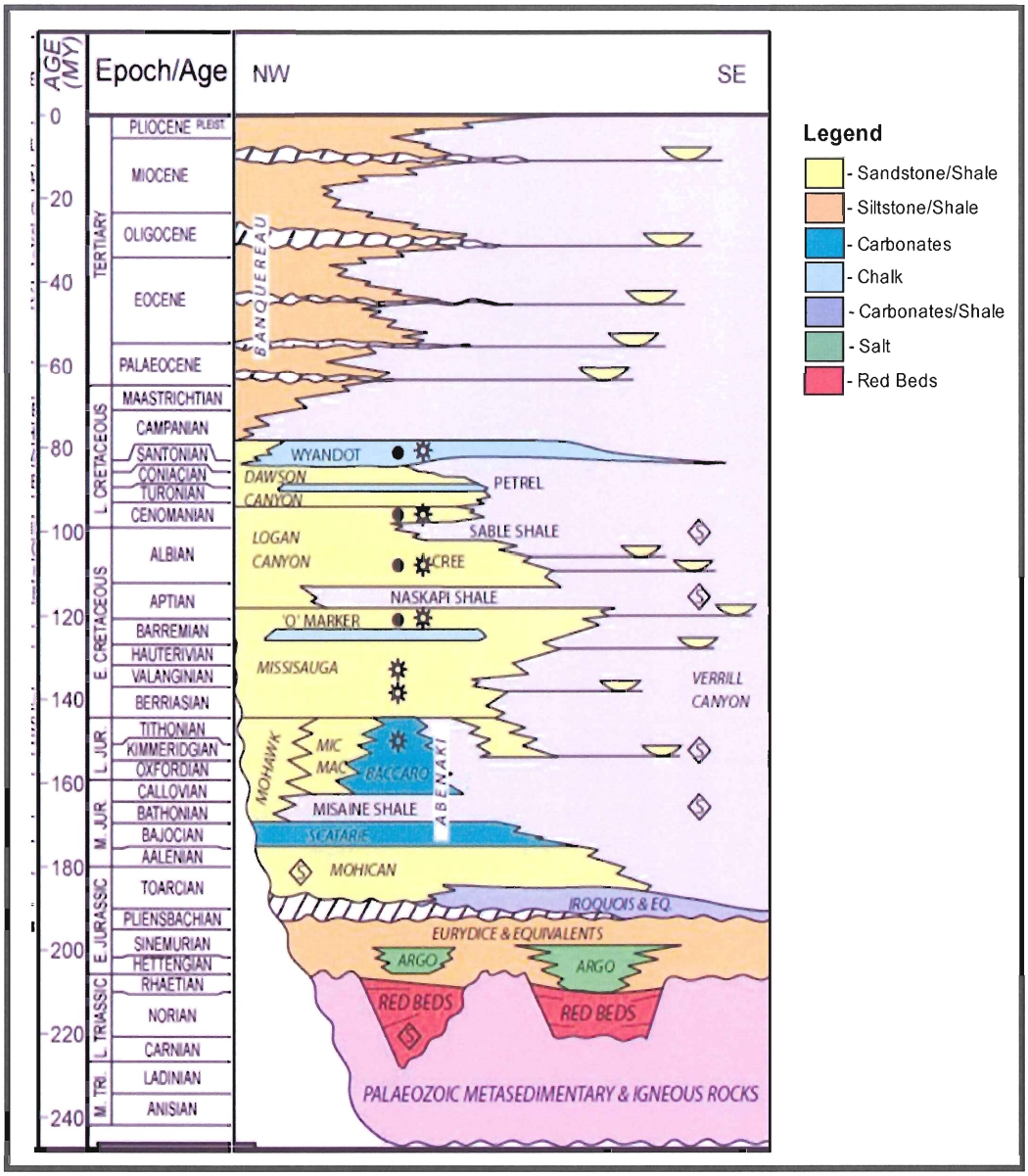

Figure 1.3: *Stratigraphic chart of the Scotian basin (Modified from Wade et al. 1995; Time scale from Palmer and Geissman, 1999).*

Following the deposition of the Mohican Formation came the deposition of the Bajocian-Tithonian Abenaki Formation which interfingers with the Mic Mac Formation.

This formation is associated with a period of basin subsidence and sea level rise. The Abenaki Formation contains the Scatarie, the Misane, and the Baccaro members. The Scatarie Member is predominantly oolitic limestone of Bajocian age, and directly overlies the Mohican Formation. The Misane Member is a transgressive shale with low organic content. The Baccaro Member is oolitic limestone and shale which formed in carbonate bank, reef and platform environments along the La Have platform.

The Mic Mac and Mohawk Formations are primarily siliclastics and are approximately equivalent in age to the Abenaki Formation. The Mic Mac Formation is ~55% shale and siltstone, 35% sandstone, and 10% carbonate, and is Callovanian to Tithonian in age and is believed to have shaled out by the slope. It is associated with the progradation of continental sediments into the basin, and consists of channel and fluvial sands that distally interfinger the marine shales of the Verrill Canyon Formation in the seaward direction. The Mohawk Formation is predominantly sandstone, and is interpreted as the more landward facies of the Mic Mac Formation.

The basinward equivalent to the Abenaki, Mic Mac, and Mohawk Formations is the Verrill Canyon Formation that ranges in age from Callovian to Barremian. This unit interfingers the Abenaki Formation, and the overlying Missisauga Fomration. It is composed primarily of organic rich shale, with minor silty to sandy beds, and is a possible source rock for the region.

The Abenaki, Mic Mac, and Mohawk Formations are all overlain by the Berriasian to Barremian Missisauga Formation which is primarily thick sandstone deposits of deltaic carbonate shoal origin that grade into thinner more shale-rich deposits down slope. This unit varies greatly in thickness throughout the Scotian Basin and

reaches more than 2000 m in regions such as the Sable sub-basin. The more coastal parts of the Missisauga Formation were deposited in an alluvial plain environment while the more distal regions were deposited in a marine shelf environment. This formation also includes a limestone member of approximately lower Barremian age that gives a strong seismic reflection, the O-marker.

Following the Missisauga Formation came the deposition of the Logan Canyon Formation. This unit is Aptian to Cenomanian and consists of shale to sandstone-shale layers deposited in a coastal-shelf plain and shallow marine environment. As the unit advances seaward there is a facies change from sandy to more shaley. The Logan Canyon Formation contains two distinct shale tongues, the Aptian Naskapi shale, and the Late Albian Sable Shale.

The Dawson Canyon Formation overlies the Logan Canyon Formation, and is Cenomanian to Santonian in age. The formation is primarily marine shales with thin siltstone, sandstone and limestone beds. Within the Dawson Canyon Formation is a remarkably continuous member of limestone beds of Turonian age, the Petrel Member. The Late Cretaceous saw a period of sea level rise. This allowed the deposition of the chalky mudstones of the Wyandot Formation on top of the shales of the Dawson Canyon Formation. This Santonian to Campanian chalk unit causes a strong seismic reflection.

On top of the Wyandot Formation rests the Banquereau Formation that contains the entire sedimentary package from Campanian to recent. The lithologies of this formation are mainly mudstones that grade upwards into sandstones and conglomerates in certain regions of the Scotian Basin. There are regional variations in thickness in the

Banquereau, and numerous unconformites are associated with sea level fluctuations during deposition.

1.5 Thesis outline

This study was conducted as there is a need for better understanding of the Scotian Slope's complex geology, particularly in the less extensively studied regions westward of the Sable sub-basin. The work done in this study was divided between analogue model interpretations, seismic interpretations, and thermal and petroleum systems modelling with an emphasis on the latter. The goal was to use the data from the analogue models and seismic images to define and create a thermal and petroleum systems model of the specific region outlined by seismic lines 1400, 5100, 5300, and 88-1a in and surrounding the eastern portion of the Shelburne sub-basin.

In order to clearly and efficiently present the procedures used and results obtained during this research project the remainder of the thesis is organized in the following manner:

- Chapter 2 focuses on the structural and stratigraphic interpretation of four seismic profiles from the regions in and surrounding the Shelburne sub-basin. Also presented is the basic information about the seismic data acquisition, and the seismic data processing done to create the seismic images.
- Chapter 3 focuses on the results of the thermal and petroleum systems model including possible petroleum systems and heat-flow predictions surrounding large salt diapirs. This chapter also includes input parameters for the model and the model configuration.

- Chapter 4 includes a discussion of results from seismic interpretations, petroleum systems modelling, and heat-flow modelling with suggestions for future models and a design for future heat-flow measurements to be taken in July 2008.
- In Chapter 5 conclusions on thermal and petroleum systems modelling are given.
- Appendix A includes interpretations of analogue model Experiment 5-7, as well as a structural restoration of the model. This section also describes the concept and procedures of analogue modelling used to create the model, as well as a basic introduction to salt tectonics on passive margins.
- Appendix B contains in depth thermal and petroleum systems modelling procedures and further information on input parameters.

Chapter Two: Seismic data interpretation

2.1 Location of interpreted lines and wells

The seismic lines interpreted are all located on the Scotian Slope. They form the perimeter of the study area for thermal and petroleum systems modelling aspect of this project, and include GX Technologies NovaSPAN lines 1400, 5100, and 5300, as well as Lithoprobe line 88-1a (Fig. 2.1). Lines 5300 and 5100 are strike lines running parallel to the strike of the Scotian slope. Line 5300 is located a few tens of kilometers seaward of the shelf-break, with line 5100 located at about the seaward limit of the slope. Lines 1400 and 88-1a are dip lines, and cut both 5300 and 5100 as they cross the Scotian Slope.

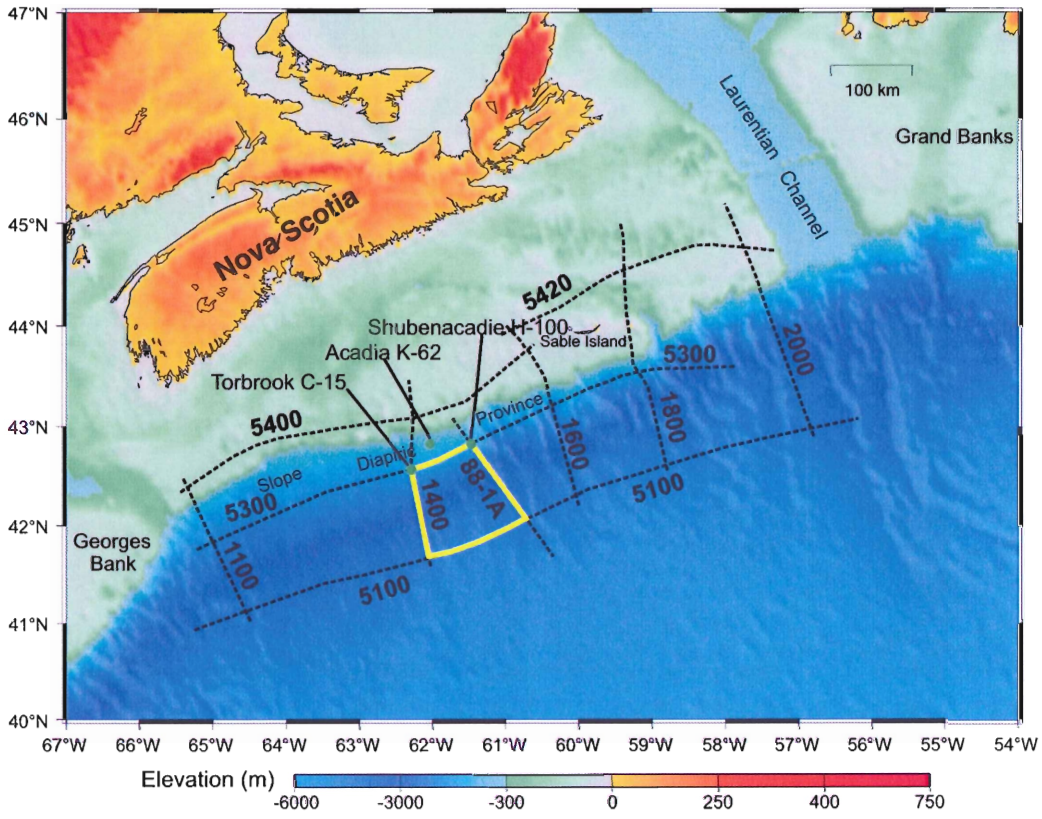

Figure 2.1: *Image of NovaSPAN lines and Lithoprobe line 88-1a in the Scotian Basin. Interpreted seismic lines forming the perimeter of the study area are highlighted in yellow. Green dots represent wells used in this study; Torbrook C-15, Acadia K-62, and Shubenacadie H-100, respectively east to west (modified from Wu Yue, personal communication).*

2.2 Seismic data acquisition and processing

The GX Technologies NovaSPAN regional 2D seismic data set was collected by a 9 km long, 360 channel streamer (Shimeld and Wade, 2005). The data were processed using free surface multiple elimination and Kirchoff pre-stack depth migration techniques. Initial seismo-stratigraphic interpretations of these lines were done by Shimeld and Wade for GX technologies NovaSPAN report (Shimeld and Wade, 2005).

Lithoprobe line 88-1a was also interpreted as part of the data set. This line was originally processed using post-stack migration in the time domain, however two sections have been reprocessed by Yue Wu at Dalhousie University (Wu, 2007). The section from Shot Point (SP) 3010 to SP 3489 was migrated using pre-stack time migration on the common offset plane, while the section from SP 3700 to SP 4356 was migrated using pre-stack time migration on the equivalent offset plane. The entire line was then converted to depth using a velocity model from wide angle seismic data (Yue Wu, personal communication, 2007).

2.3 Methods of interpretation

Interpretations of the four seismic profiles bounding the study area for thermal and petroleum systems modelling were done using Kingdom Suite 8.1 software. Thirteen horizons were picked, representing specific formation tops and age boundaries within the Scotian Slope (Table 2.1).

The primary constraints on interpretations were correlations from the Shubenacadie H-100, Torbrook C-15, and Acadia K-62 wells (Fig. 2.1). General lithological and stratigraphic data from these wells were collected from the publicly available well reports at the CNSOPB in Dartmouth Nova Scotia, as well as from the

	Horizon Color	Horizon Name	Age Boundary
1	Red	Banquereau_1	Recent (0 Ma)
2	Green	Banquereau_2	Mid Pliocene (3.6 Ma)
3	Magenta	Banquereau_3	Top Oligocene (23.03 Ma)
4	Deep Blue	Banquereau_4	Top Eocene (33.9 Ma)
5	Light Blue	Banquereau_5	Top Paleocene (56.5 Ma)
6	Orange	Wyandot	Campanian (~75 Ma)
7	Green	Logan_Canyon	Cenomanian (~95 Ma)
8	Yellow	Missisauga	Top Hauterivian (~130 Ma)
9	Brown	Baccaro	Top Tithonian (~145 Ma)
10	Blue	Misane	Top Callovian (~161 Ma)
11	Magenta	Scatarie	Top Bajocian (~168 Ma)
	Bright Green	Argo_Salt	Lower Jurassic (~190 Ma)
12	Red	Basement	Upper Triassic (~ 210 Ma)

Table 2.1: *Horizons of interest and associated information (Moir et al., 2007)*

Natural Resources GSC BASIN database (Table 2.2). A secondary constraint on the selection of horizons where well data were not available was the initial stratigraphic interpretation of the lines done by Shimeld and Wade (2005) for GX Technologies. Their interpretations included horizons representative of general age boundaries and formation tops. However, reinterpretation was necessary as many of the horizons picked were not continuous across the entire seismic profiles which is a requirement for 4D modelling.

Formation tops were correlated from the well data to the seismic images, and the formation tops were assigned to prominent reflectors at the proper depths. These reflectors generally correlated well with the picks made by Wade and Shimeld, but some picks had to be adjusted to fit strong reflectors and well data, as well as the specific formation tops and age boundaries desired for the petroleum systems modelling portion of this project. For the horizons at depths not penetrated by any wells the horizons picked were based on prominent reflectors and the interpretations by Shimeld and Wade (2005), as well as the literature on the Scotian Basin.

Shubenacadie H-100 Well						
Marker Name	**Corresponding Horizons**	**Top Depth**	**Base Depth**	**Thickness (m)**	**Bottom Age (Ma)**	**Lithology**
Sediment Surface	Banquereau_1	-	1476.5	0	0	-
Banquereau Fm.	Banquereau_1	1476.5	2988.39	1582.5	33.9-0 (Recent)	Shale, interbedded quartzose sand
Banquereau Fm.	Banquereau_3	2988.39	3703	714.61	75-33.9 (Top Eocene)	Shale, minor chalk beds
Wyandot Fm.	Wyandot	3703	3795	92	85-75 (Campanian)	Chalk
Dawson Canyon Fm.	-	3795	4000	205	95-85 (Santonian)	Shale and mudstone, minor chalk beds
Shortland Shale	Logan_Canyon_2116	4000	4200	200	~125-95 (Cenomanian)	Shale, minor sand stringers
Torbrook C-15 Well						
Marker Name	**Corresponding Horizons**	**Top Depth**	**Base Depth**	**Thickness (m)**	**Bottom Age (Ma)**	**Lithology**
Sediment Surface	Banquereau_1	-	1674.5	0	0	-
Banquereau Fm.	Banquereau_1	1674.5	2962	1287.5	20-0 (Recent)	Interbedded shale, clay and siltstone
Banquereau Fm. (Tertiary 33)	-	2962	3260	298	23.03-20 (Miocene)	Interbedded shale, clay and siltstone
Banquereau Fm. (Tertiary 30)	Banquereau_3	3260	3488	228	33.9-23.03 (Top Oligocene)	Shale
Banquereau Fm. (Tertiary 20)	Banquereau_4	3488	3600	112	?-33.9 (Top Eocene)	Shale
Acadia K-62 Well						
Marker Name	**Corresponding Horizons**	**Top Depth**	**Base Depth**	**Thickness (m)**	**Depositional Ages (Ma)**	**Lithology**
Sediment Surface	Banquereau_1	-	866.3	0	0	-
Banquereau Fm.	Banquereau_1	866.3	2593.4	1727	75-0 (Recent)	Shale, Clay, minor sandstone
Wyandot Fm.	Wyandot	2593.4	2620.1	26.7	85-75 (Campanian)	Chalk
Dawson Canyon Fm.	-	2620.1	2714.4	94.3	95-85 (Santonian)	Shale, minor limestone
Petrel Mem. (~equals Shortland Shale)	~Logan_Canyon	2714.4	2778	63.6	130-95 (Cenomanian)	Shale, topped by thin limestone
Roseway (~equals O-marker)	~Missisauga	2778	3306	528	145.5-130 (Top Hauterivian)	Limestone, minor dolomite
Top Abenaki Fm.	Baccaro	3306	4086	780	161.2-145.5 (Top Tithonian)	Oolitic limestone, minor dolomite
Misaine Mem.	Misane	4086	4304	218	167.7-161.2 (Top Callovian)	Shale, minor siltstone/sandstone
Scatarie Mem.	Scatarie	4304	4950	646	172-167.7 (Top Bajocian)	Oolitic limestone, minor sandstone
Mohican equivalent		4950	5287.4	337	~180-172 (Top Aalenian)	limestone, minor shale/ sandstone

Table 2.2: *well data from a) Shubenacadie H-100, b) Torbrook C-15, and c) Acadia K-62 wells. Horizons picked in the seismic interpretations corresponding to marker horizons in the wells are shown.*

Once selected, the reflectors of interest were followed across the entire seismic profiles. Reflectors representing the same ages and formation tops in the lines were correlated throughout the study area by matching the depths to reflectors at the intersections of the lines. Thirteen consistent horizons were correlated across all four seismic profiles. As laterally continuous reflectors are required for input into PetroMod, horizons were picked across the entire seismic lines, and their locations had to be inferred where reflectors were weak or imaging was poor.

All horizons were inferred from either well data or the initial interpretations by Shimeld and Wade (2005) except for the Argo salt horizon. The Argo salt horizon was selected to outline the numerous complex salt bodies throughout the Scotian Slope. Salt bodies make seismic imaging challenging because they generally have a much higher acoustic velocity than the surrounding sediments. Salt bodies in seismic images are represented by a lack of reflectors, or by weak disorganized reflectors rather than the generally parallel, horizontal reflectors of the sediments.

2.4 Lithological and stratigraphic interpretations

The basement, underlying the "Basement" horizon, was difficult to pick as imaging was poor due to the thick sedimentary cover and great depths. Imaging of the basement was particularly poor in regions overlain by salt, specifically on lines 88-1a and 1400. The basement is composed of pre-Triassic crystalline rocks, forming a series of topographic highs and lows in a jagged terrain. It is covered by syn-rift sediments of the Eurydice Formation, and the salt of the Argo Formation (the Argo_Salt horizon). The Argo salt was deposited during the Early Jurassic.

The first post-rift horizon interpreted is the "Scatarie" horizon, which corresponds to the top of the Scatarie Formation. The cause for the strength of the reflector in the seismic images is likely the change from the primarily shale Misane Member to the underlying limestones of the Scatarie Formation (Moir et al., 2007 (Acadia K-62 well); and Wade and MacLean, 1990). The rocks underlying the "Scatarie" horizon are primarily oolitic limestones with lesser quantities of fine grained sandstone (Moir et al., 2007 (Acadia K-62 well)).

The "Misane" horizon of Top Callovian age lies within the Abenaki Formation. It represents the top of the Misane Member. The rocks underlying this horizon are likely transgressive shales with minor interbedded siltstones and fine-grained sandstones (Wade and MacLean, 1990). The Misane Member has a small amount of organic material within it and is a potential source rock. The strong reflector at this boundary is likely caused by the transition from the limestones of the Baccaro member to the shales of the Misane Member.

The "Baccaro" horizon represents the Top Tithonian boundary, as well as the top of the Abenaki Formation. Beneath this horizon the Acadia K-62 well shows beds of oolitic limestones with minor amounts of dolomite that continue for ~780 m until the contact with underlying Misane Member (Moir et al., 2007). The limestone corresponds to the Baccaro Member, but no sandstone siliclastics of the equivalent Mic Mac Member were drilled.

The Cretaceous section begins with a sandstone unit which likely grades into a more shale-rich unit seaward (Wade and MacLean, 1990). This layer belongs to the Missisauga Formation and equivalents, and is topped by a strong reflector, the

"Missisauga" horizon, which corresponds approximately to the Top Hauterivian Boundary. The Acadia K-62 well shows that underlying the "Missisauga" horizon is a relatively uniform shale unit with a few thin limestone beds and sand stringers. The strong reflector associated with the "Missisauga" horizon is the result of a specific strong limestone reflector, the O-marker (Wade and MacLean, 1990). This boundary is located near the top of the Missisauga Formation, and near the transition to the Logan Canyon Formation.

The "Logan_Canyon" horizon is of Cenomanian age, and corresponds with the top of the Logan Canyon Formation. In the interpretations of lines 5300 and 88-1a, the "Logan_Canyon" horizon corresponds to the Top Shortland Shale marker in the Shubenacadie H-100 well at a depth of ~4000 m, which is a seaward equivalent to the Logan Canyon. The Shortland Shale is likely to be composed of landward sandstones with a seaward transition into a more shaley facies (Wade and MacLean,1990). The Shubenacadie H-100 well shows that this unit contains primarily shale with minor sand stringers, and thus corresponds to a more basinward equivalent of the Logan Canyon Formation.

The next horizon, the Wyandot marker, is the top of the Lower Campanian strata. This strong reflector is associated with the Wyandot Chalk, which in the Shubenacadie H-100 well is a 65 m thick chalk unit underlain by the Dawson Canyon Formation. The Dawson Canyon Formation contains primarily marine shales, however minor chalk (Moir et al., 2007 (Shubenacadie H-100 well)), and limestone beds (Moir et al., 2007 (Acadia K-62 well)) are present.

Overlying the "Wyandot" horizon is the Banquereau Formation which includes horizons Banquereau 1-5. The Banquereau Formation consists almost entirely of mudstones and shales with an upward transition into interbedded siltstones and fine-grained quartzose sandstones (Moir et al., 2007 (Shubenacadie H-100 well and Torbrook C-15 well)). The numerous prominent reflectors in this sequence are a result of the transition from mudstones to sandstones/siltstones which reflect the many transgression/regression cycles during deposition (MacLean and Wade, 1990). Horizon "Banquereau_4" was correlated in both the Shubenacadie H-100 and the Torbrook C-15 wells to the Top Eocene boundary, and horizon "Banquereau_3" was correlated in the Torbrook C-15 well to the Top Oligocene boundary (Moir et al., 2007). Above "Banquereau_3" are Quaternary sediments, primarily clays, with minor sand and silt deposits.

2.5 Structural interpretations

2.5.1 Line 88-1a

Lithoprobe line 88-1a showss an abundance of salt and shows four large vertical diapirs that will be referred to as D1, D2, D3, and D4, landward to seaward (Fig. 2.2). These diapirs extend from the basement to just past the Top Campanian boundary, the "Wyandot" horizon. Diapir D1 comes within ~1000 m of the surface. Diapir D2 appears to be squeezed and contains a small salt tongue (C1) overlying the Campanian strata. The diapirs in line 88-1a are slightly taller than those in line 1400, bringing them within 1000-1500 m of the surface. A thin layer of autochthonous salt is present between the diapirs resting on the basement, and continues landward up the basement high. The basement is poorly imaged under the salt and its location has been inferred. Seaward of the salt

diapiric region the basement shows faulting and tilted fault blocks that persist farther seaward beyond the study area boundaries (past cross line 5100), where they are found at greater depth and are filled with syn-rift sediments (Wu, 2007).

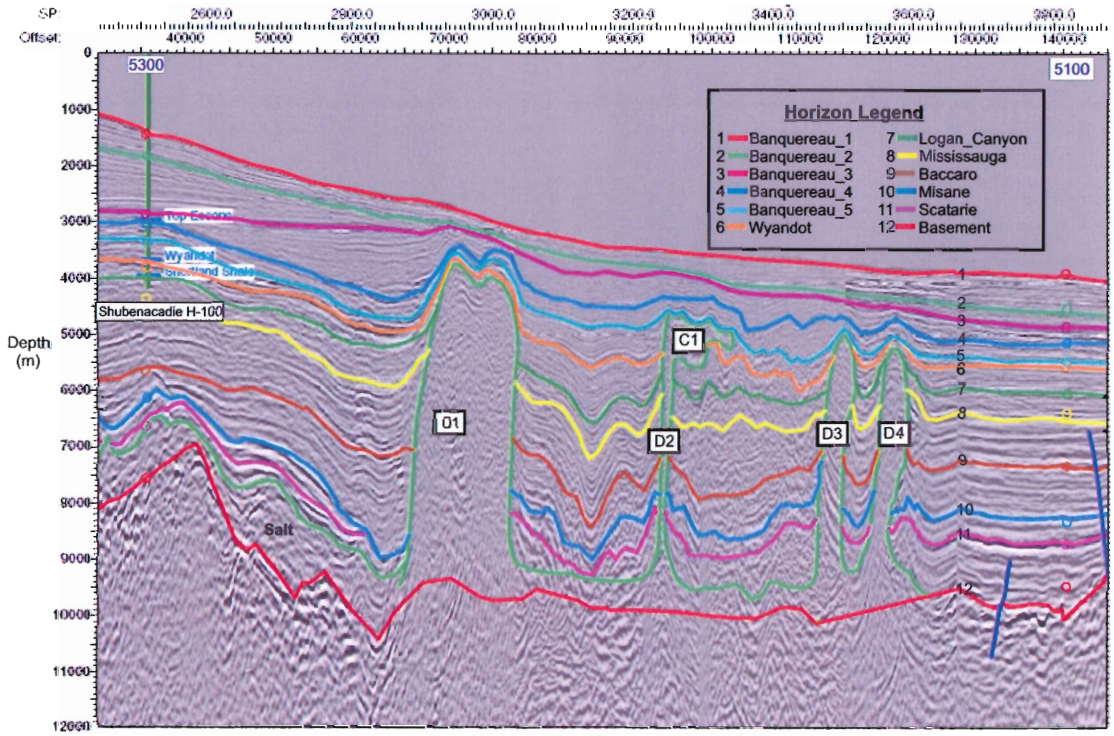

Figure 2.2: *Seismic interpretation of line 88-1a with four large diapirs, D1-D4, and one canopy, C1. Cross lines intersect at locations of blue line numbers.*

2.5.2 Line 1400

GX Technologies line 1400 contains a series of vertical diapirs of differing sizes, including four large diapirs labeled D1-D4 landward to seaward respectively. The largest diapir, D1, pierces the Campanian "Wyandot" marker horizon, and comes within ~1500 m of the surface (Fig. 2.3). Autochthonous salt is located along the basement between the diapirs and continues landward up the basement steps. Under shotpoint (SP) 2300 the sedimentary strata thicken seaward against the flanks of the large diapir (D2) and are likely growth strata associated with an explusion rollover formed during the formation of the diapir (Appendix A). The basement is obscured by salt in much of the

profile, however, salt does not extend seaward of shotpoint 1500, allowing for more accurate basement interpretations. The basement in this region contains minor fault blocks from shotpoint 1400 to 1100. These fault blocks are a result of extension associated with rifting during the Late Triassic continental breakup.

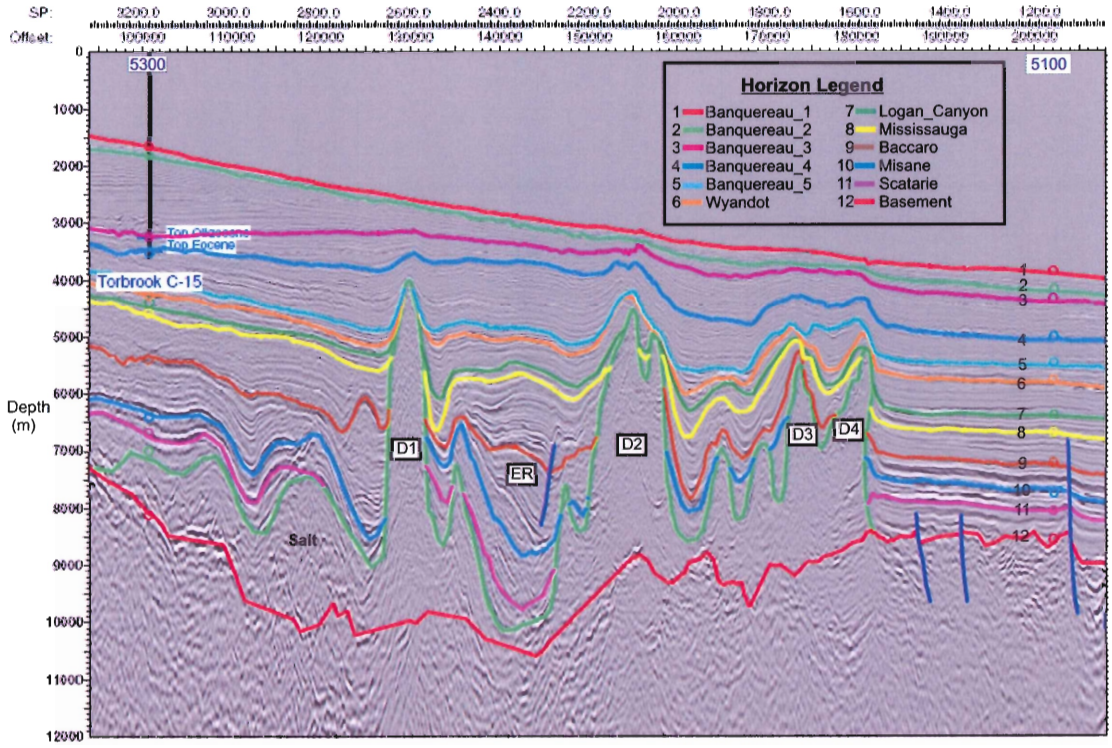

***Figure 2.3**: Seismic interpretation of line 1400 with large diapirs D1-D4. Expulsion rollover is marked with ER. Cross lines intersect at locations of blue line numbers.*

2.5.3 Line 5100

Line 5100 runs along strike with the continental margin at the base of the continental slope (Fig. 2.1). This line is seaward of any salt, and thus imaging of the basement is good (Fig. 2.4). The sedimentary strata in this region are relatively undeformed and form parallel layers. Basement in the region is jagged, yet not highly faulted. Further east of the study area, past cross line 1600 there is a section of tilted basement fault blocks filled with syn-rift sediments.

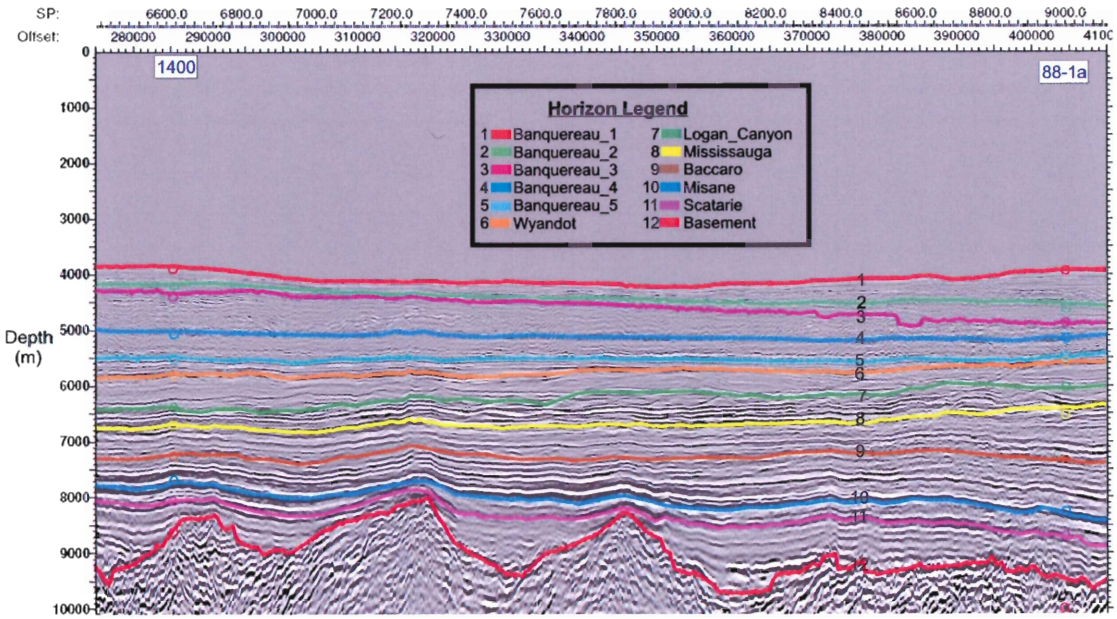

***Figure 2.4**: Seismic interpretation of line 5100. Cross lines intersect at locations of blue line numbers.*

2.5.4 Line 5300

Line 5300 runs along strike with the Scotian Margin just seaward of the landward limit of the Scotian slope. This profile contains thick, relatively undeformed parallel strata (Fig. 2.5), much thicker than in the seaward strike line 5100 (Fig. 2.4). The basement is overlain by a relatively thin layer of salt, and likely represents the landward limit of the Argo salt. The basement is jagged and well imaged.

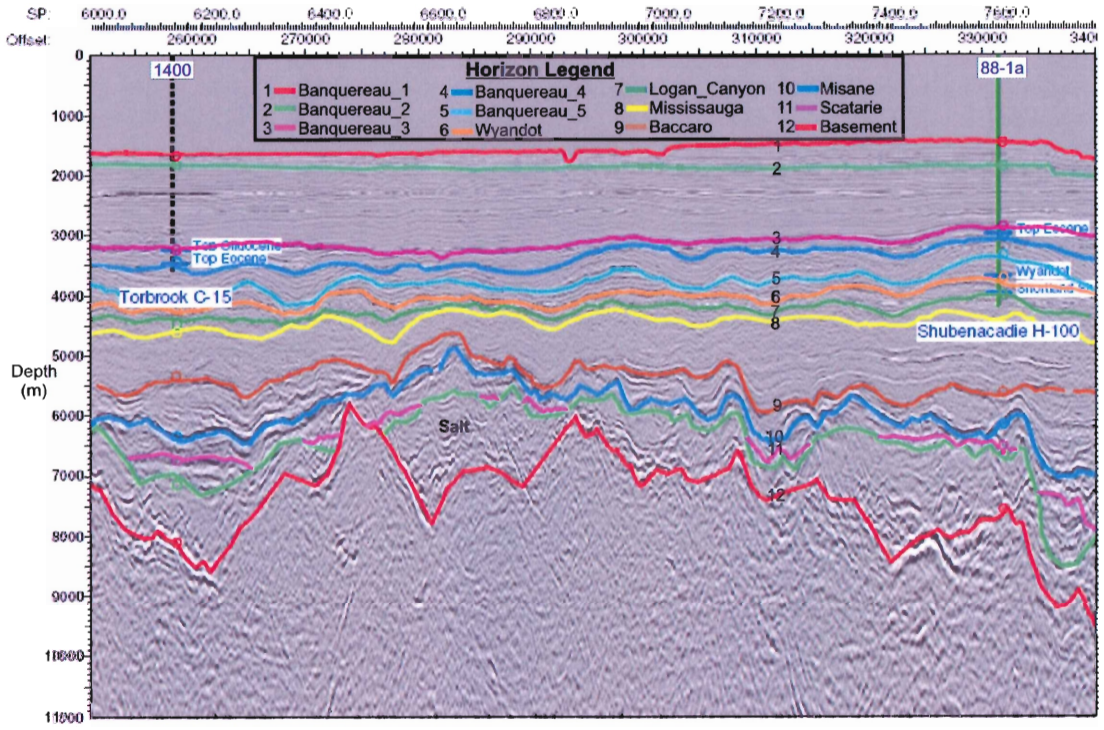

***Figure 2.5**: Seismic interpretation of line 5300. Cross lines intersect at locations of blue line numbers.*

Chapter Three: Thermal and Petroleum Systems Modelling

3.1 Introduction to 4D modelling

3.1.1 Basis for 4D modelling

A 4D model of the region bounded by GXT lines 1400, 5100, 5300, and Lithoprobe line 88-1a (Fig. 2.1) was created using PetroMod 10 software to predict surface heat-flow and show the effects of salt diapirs on the heat-flow. The model is also used to determine the petroleum systems potential of the study area. The surface heat-flow calculated in the model will be used to constrain locations for heat-flow measurements to be taken in July of 2008. Well data, analogue models, seismic interpretations of the bounding lines, and available literature on the Scotian Basin provide constraints for modelling. For a detailed account of modelling methods and procedures refer to Appendix B.

3.1.2 Boundary assignments

To calculate present-day heat-flow and petroleum maturation and migration boundary assignments must be set in PetroMod. These include Paleo Water Depth (PWD), Sediment Water Interface Temperature (SWIT), and relative Heat-Flow (HF), each for the entire geologic history of the model (Fig. B.1). Geological knowledge and vitrinite reflectance data from the Acadia K-62 well (Avery, 2004) were used to make and calibrate the heat-flow curve (Fig. B.2). The %Ro graph does not have a commonly observed profile as the deepest vitrinite data point does not appear to agree with the rest of the data, resulting in a slight shift of the curve to the left.

3.1.3 Experiment configuration

The model configuration is derived from the depth-converted layers created from the seismic interpretations of line 88-1a, 1400, 5100, and 5300, explained in Chapter two. All formations interpreted in the seismics are present in the 4D model (Table B.4) with the addition of the Dawson Canyon and Verrill Canyon Formations and some additional facies including source and reservoir rocks as specified for petroleum systems modelling purposes (Table B.5). Salt diapirs were put in last, once all other layers were created and their properties had been assigned (Appendix B-3.6). The centre part of the block has a large uncertainty due to lack of data, and likely has artificial structure. Once all input

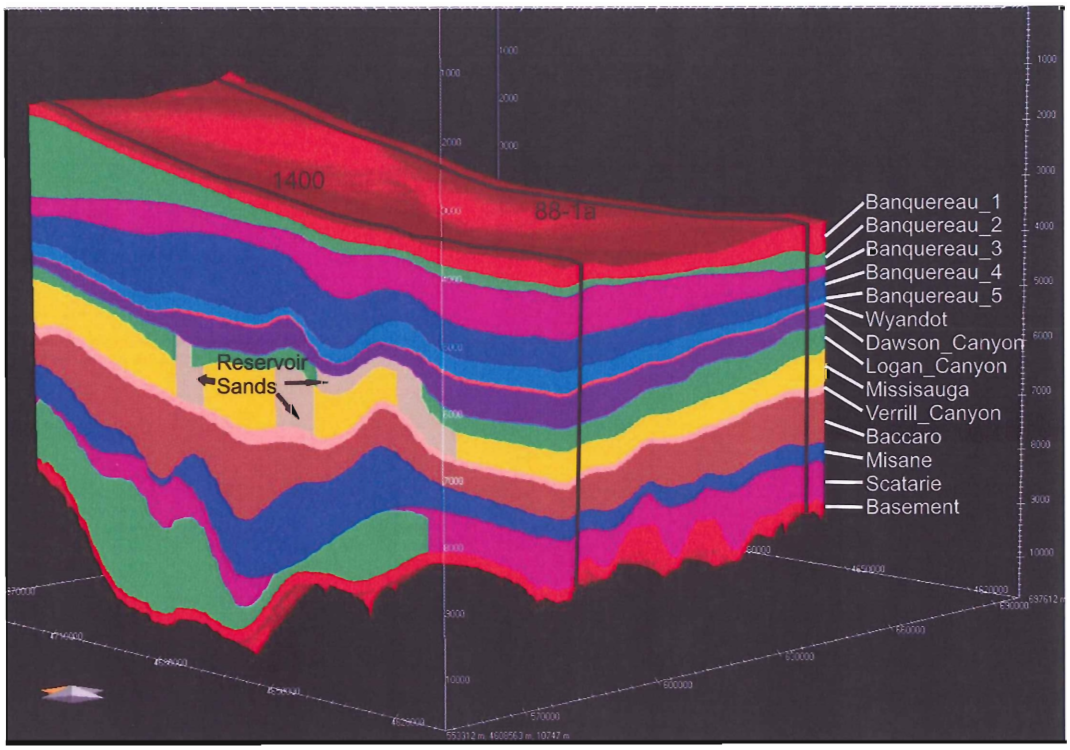

Figure 3.1: *General view of 3D model showing formations and locations of seismic line 1400 and 88-1a.*

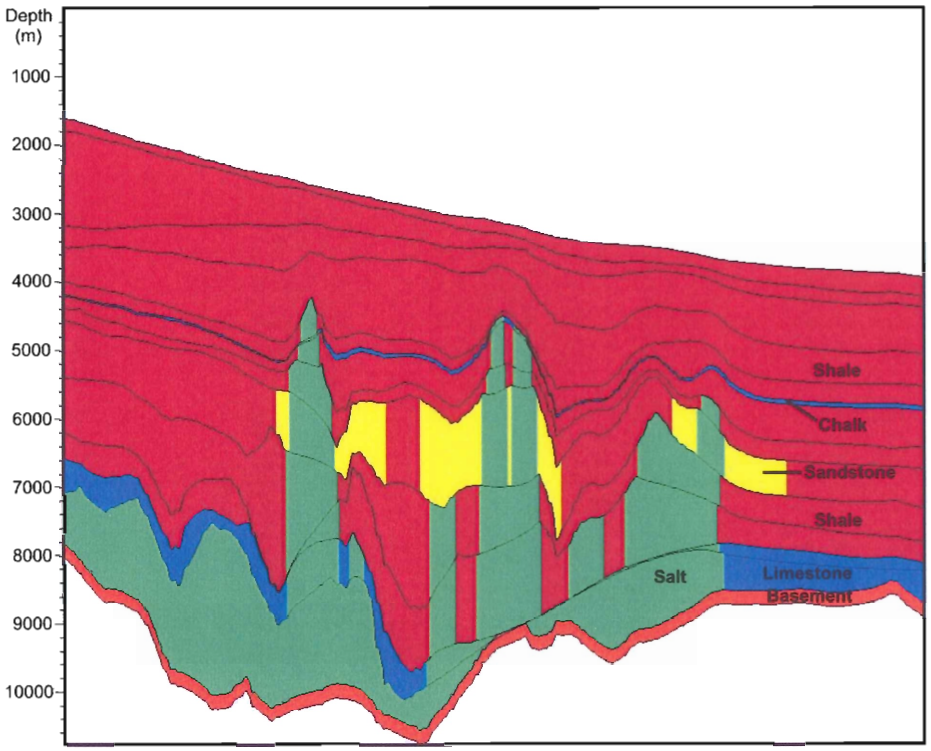

Figure 3.2: *Cross section of model along line 1400 showing salt diapirs and dominant lithologies.*

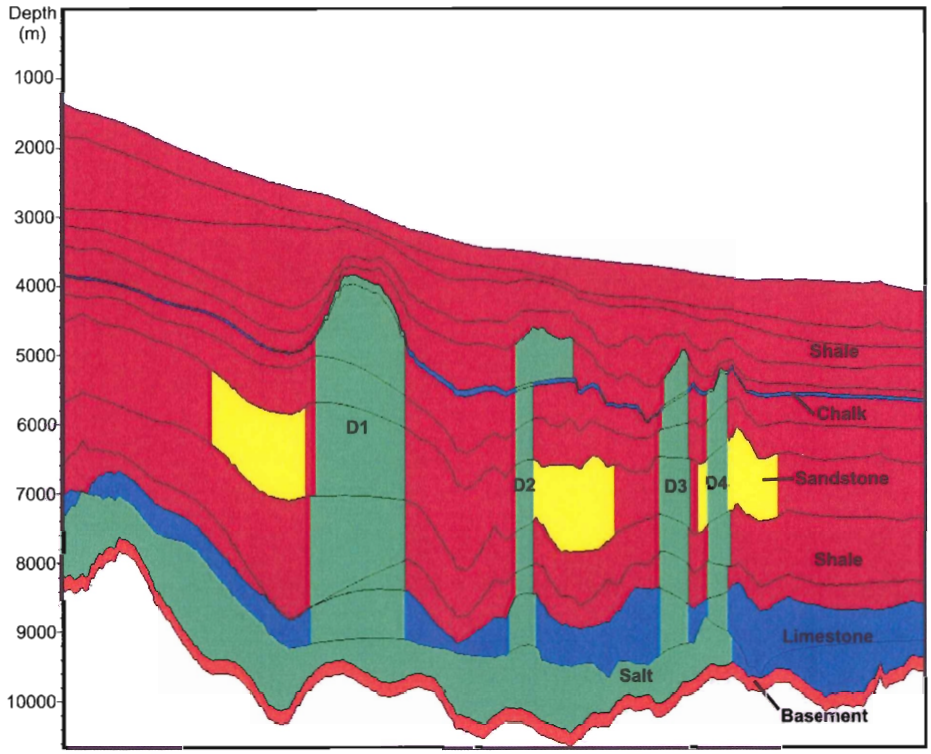

Figure 3.3*: Cross section of model along line 88-1a showing salt diapirs (D) and dominant lithologies.*

parameters were set, a simulation was run to show the evolution of the modeled region from Late Triassic to present, and to calculate surface heat-flow and petroleum potential. A general view of the model can be seen in Figure 3.1. Cross sections of the model along lines 1400 (Fig. 3.2) and 88-1a (Fig. 3.3) show dominant lithologies assigned to the model.

3.1.4 Constraining diapir evolution

In the summer of 2006, the Dalhousie Salt Dynamics Group created an analogue model entitled "Experiment 5-7" to model the evolution of salt diapirs in the Scotian Basin. As part of this thesis I have interpreted and structurally restored the model in order to gain insight on constraining the timing of diapir growth. A thorough account of the model configuration, modelling techniques, interpretations and structural restorations is included in Appendix A. The structural restoration of analogue model Experiment 5-7 shows that salt begins to flow immediately upon differential sedimentary loading atop the salt layer (Fig. 3.4). Diapir growth is found to keep pace with sedimentation as long as sedimentation remains constant and differential loading is maintained. Therefore, in the model diapirs have been set to pierce the surface of the sediment layers simultaneously with sediment deposition (Fig. 3.5).

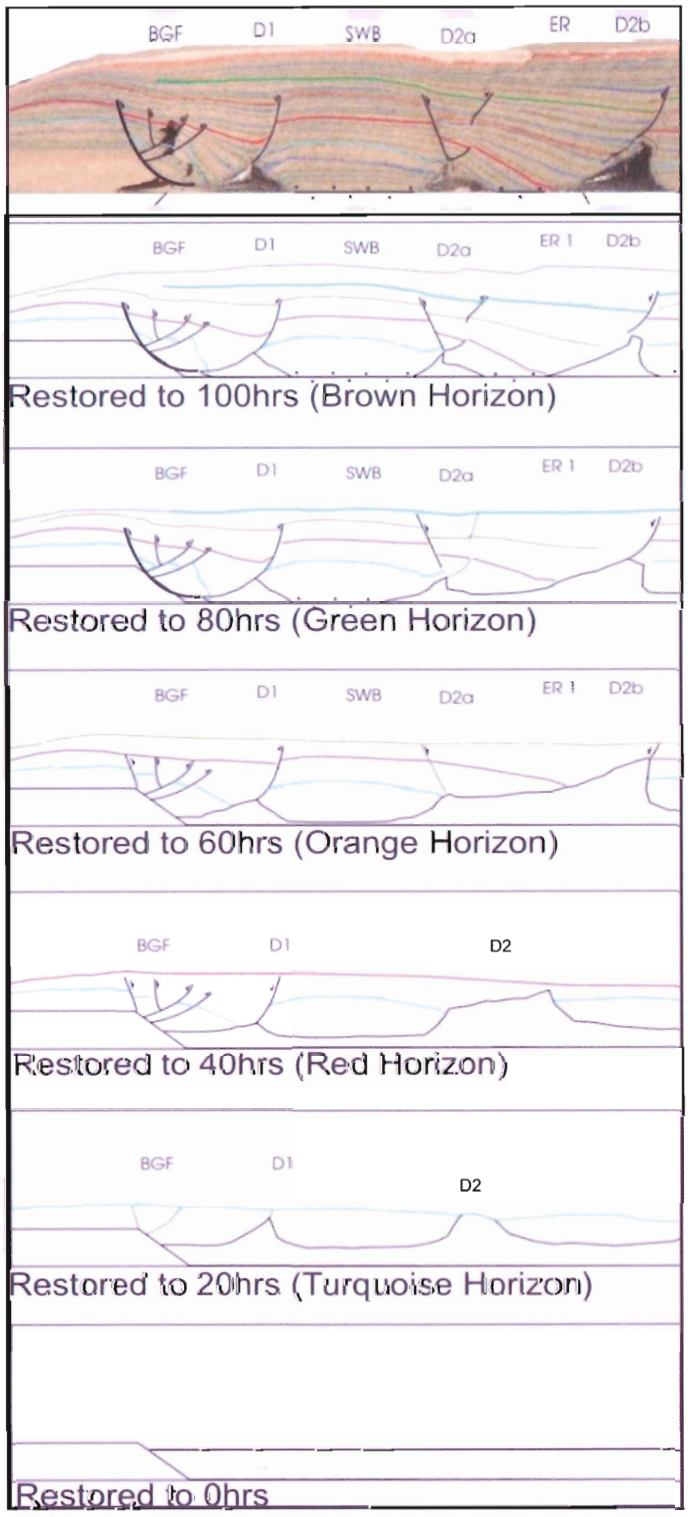

Figure 3.4: *Structural restoration of Experiment 5-7 showing diapir growth beginning as soon as sediment deposition commences. BGF=Basinward Growth Fault, D=Diapir, SWB=Salt Withdrawal Basin, KG=Keystone Graben, ER=Expulsion Rollover.*

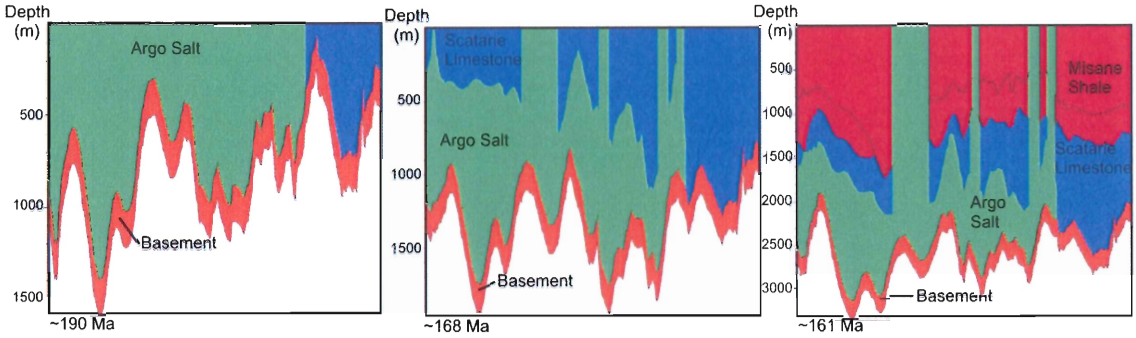

Figure 3.5: *Argo salt piercing overlying layers at the same time they are being deposited.*

3.2 Thermal modelling

The model has been used to predict present day heat-flow and temperature variations with depth. PetroMod calculates heat-flow and temperature based on the types of lithologies selected for each layer of the model and the boundary conditions the model has been assigned. Every lithology has associated properties such as density, thermal capacity and conductance that are specified within the PetroMod software. These, along with the assigned boundary conditions (Fig. B.1), ages (Table B.4) and burial depths are used by PetroMod to calculate present-day heat-flow and temperature during simulation.

3.2.1 The affect of salt on heat-flow

Salt in sedimentary basins has been found to have a pronounced affect on the heat-flow in the regions above, beneath and surrounding the salt. Salt is a much better heat conductor than most sediment with conductivity some 2-3 times higher (Yu et al., 1992). Large salt diapirs act as low thermal resistance conduits through which heat can be easily transported. This results in local thermal anomalies, as heat is transported faster from great depths to shallow depths in diapirs (Fig. 3.6). Due to the elevated heat-flow in salt, increased temperatures and heat-flow are found in sediments above salt bodies, and decreased temperatures are found beneath salt bodies.

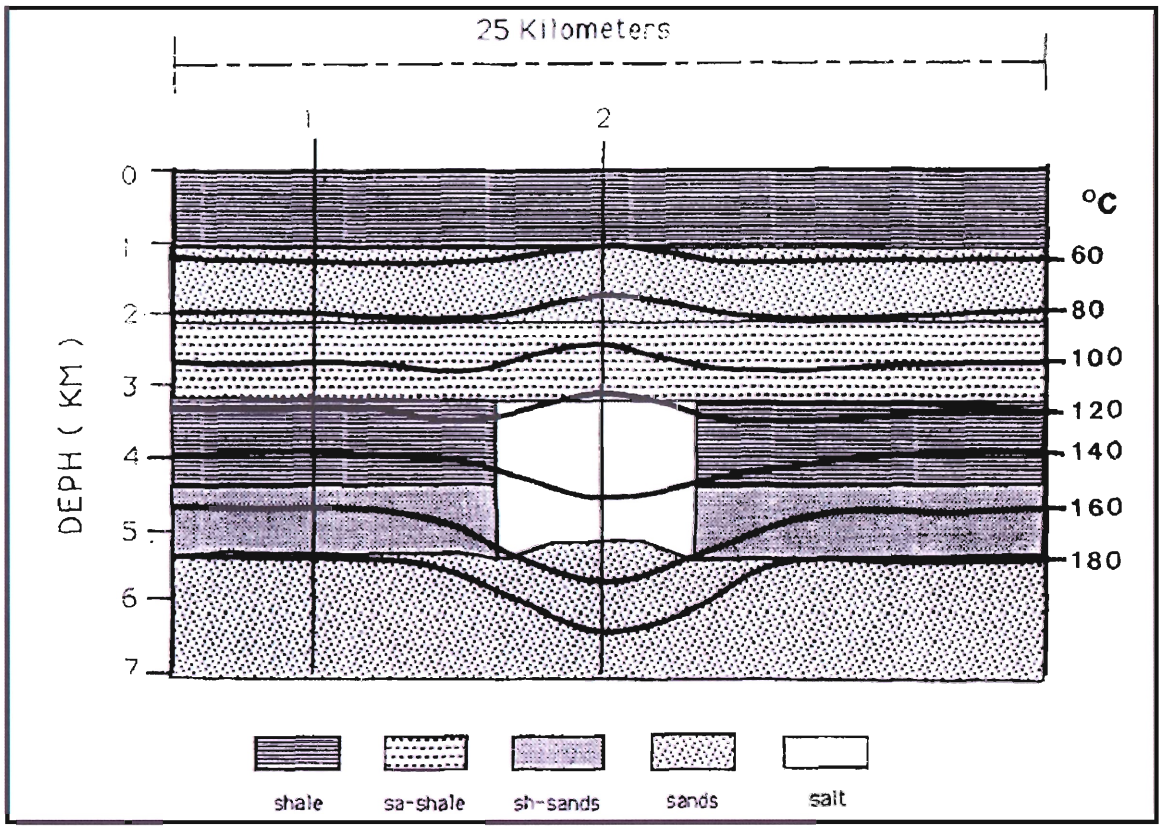

Figure 3.6: *Lateral temperature variation with respect to salt body location showing increased temperature above salt and decreased temperature beneath (Yu et al., 1992).*

3.2.2 Thermal modelling results

As predicted, the model shows significant increase in heat-flow above salt diapirs. The surface heat-flow spikes in circular patterns along the traces of seismic lines 1400 and 88-1a above the salt diapirs (Fig. 3.7). A surface view of diapir locations can be seen in Figure 3.8, and diapir heights and extents can be seen in the cross sections along the trace of line 1400 (Fig. 3.2) and 88-1a (Fig. 3.3). Surface heat-flow above diapirs reaches values of ~65-78 mW/m^2, while surrounding regions show values of only 45-55 mW/m^2 (Fig. 3.7). The highest surface heat-flow value of ~78 mW/m^2 is in the north-eastern regions of the model (Fig. 3.7) along the trace of seismic line 88-1a above D1 (Fig. 3.3).

Heat-flow within the salt diapirs is significantly higher than the heat-flow at the surface above the diapirs. Heat-flow in the diapirs is found to reach peaks of ~130 mW/m^2 (Fig. 3.9, Fig. 3.10). The highest heat-flow values are found in the tall thin diapirs, in particular diapir D2 along the trace of line 88-1a (Fig. 3.10), and the peak of the tallest diapir in line 1400 (Fig. 3.9). The wider diapirs show maximum heat-flow values of ~95 mW/m^2 near the edges that drop to ~65 mW/m^2 in the center. The sediments adjacent to and beneath the diapirs show significant decrease in heat-flow while the sediments above the diapirs show increased heat-flow.

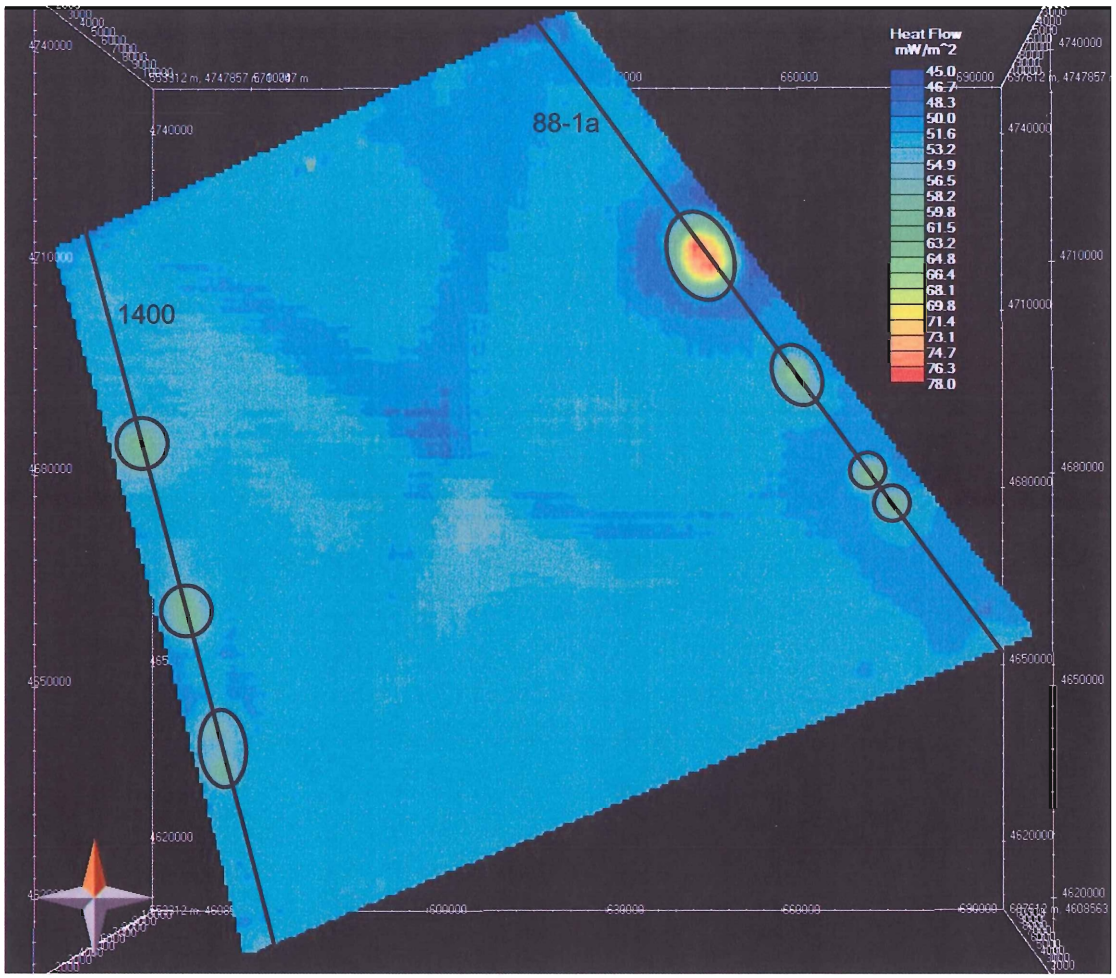

Figure 3.7: *Surface of model showing heat-flow. Regions of high heat-flow are circled in black. Orange arrow points north.*

The model shows significant lateral temperature variations in the basement layer, below the salt. Circular temperature anomalies are observed along the traces of seismic lines 88-1a and 1400 (Fig. 3.11). They record exceptionally low temperatures with respect to their surroundings and correspond with the locations of the salt diapirs (Fig. 3.8). The salt diapirs with their high thermal conductance are essentially sucking the heat out of the underlying basement and transporting it to the surface.

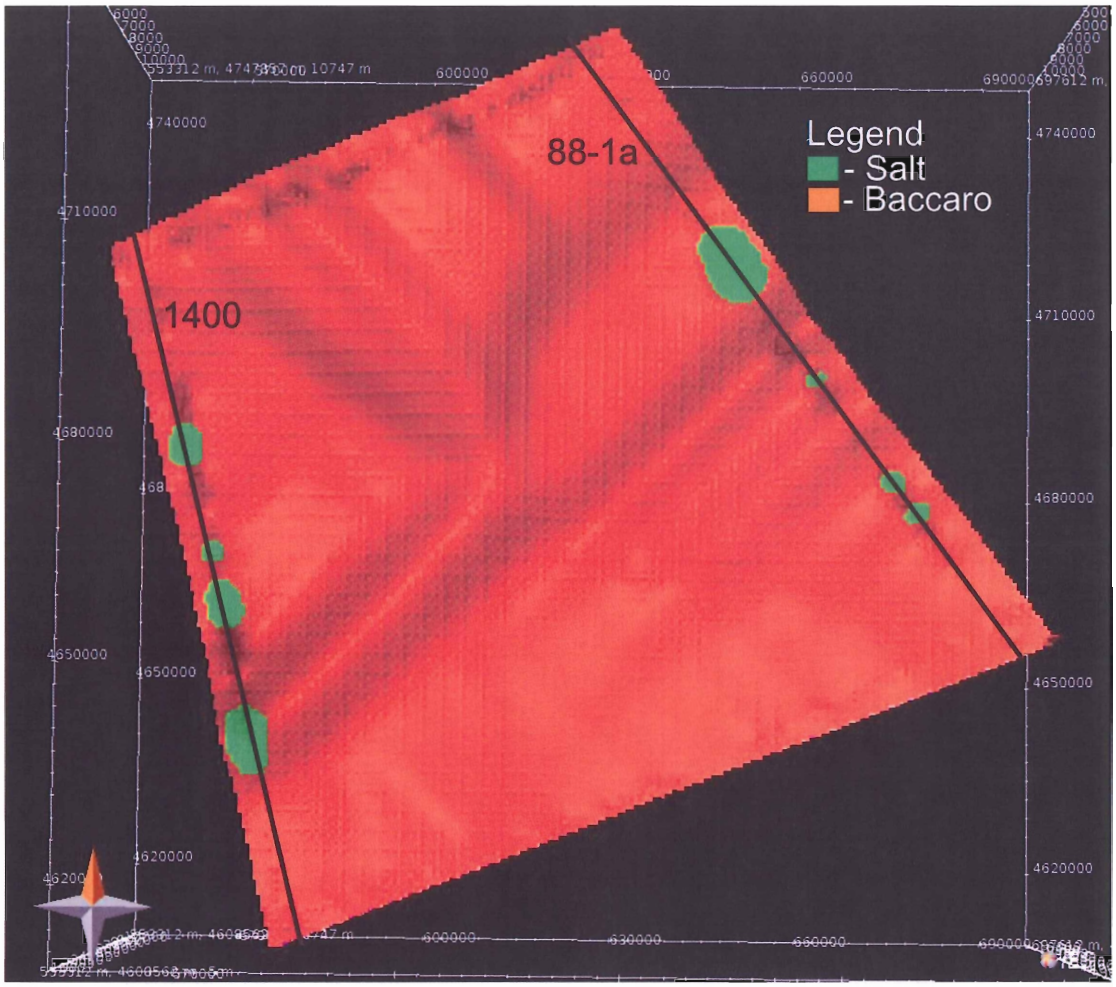

Figure 3.8: *Surface view of the Baccaro layer showing locations of major diapirs. Locations of seismic lines 1400 and 88-1a are shown in black.*

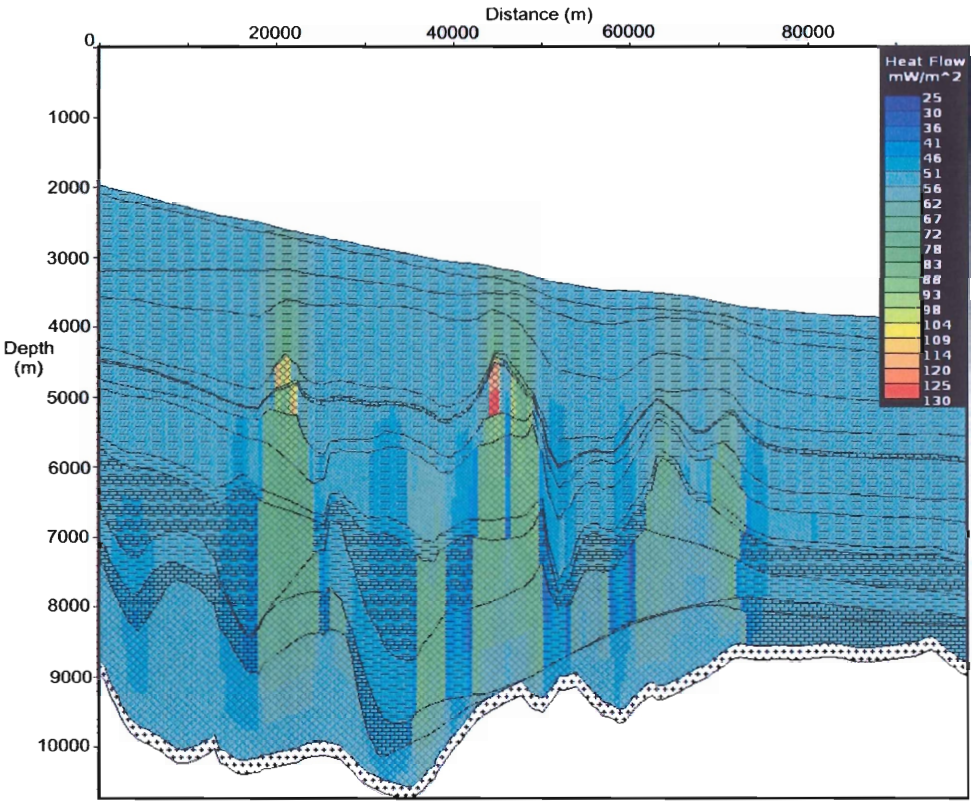

Figure 3.9: *Cross section of line 1400 showing the effect of salt diapirs on heat-flow.*

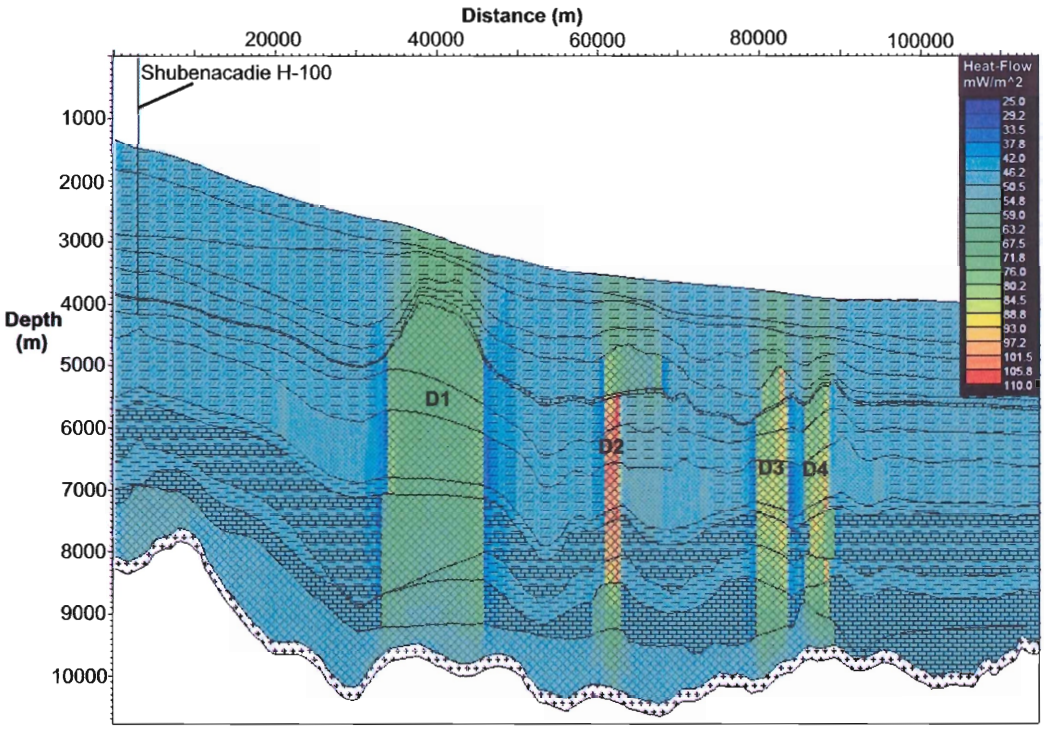

Figure 3.10: *Cross section of line 88-1a showing the effect of salt diapirs (D1-D4) on heat-flow.*

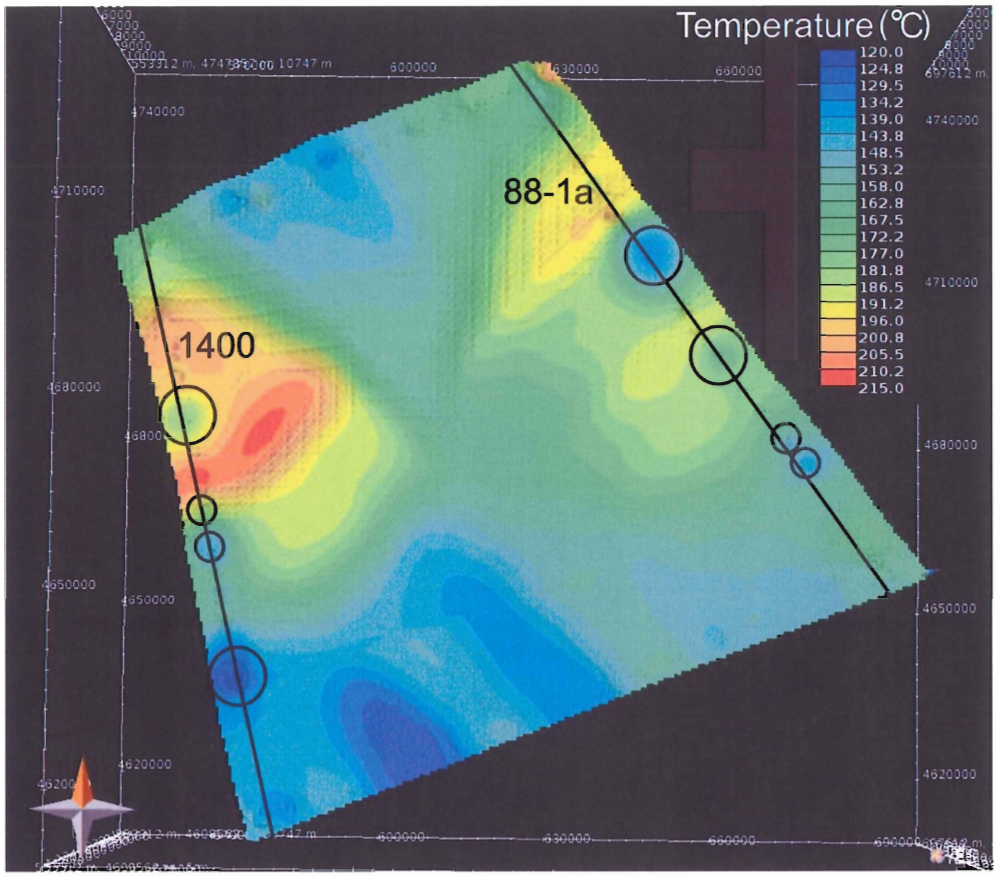

Figure 3.11: *Surface view of the basement showing temperature variations. Regions of low temperature are circled in black.*

3.3 Petroleum systems modelling

The 4D model was also built to show the petroleum system(s) potential of the study area. As there is little constraint from wells in the region, many petroleum system elements were inferred from literature on the Scotian Basin. Source and reservoir rocks are essential in defining a petroleum system. With the lack of wells on the Scotian slope these elements had to be inferred from data on the lithologies and formations of Scotian shelf. As the dominant lithology for most of the study area is shale which acts as a good seal rock, no particular layers needed to be specified as seal rocks.

The Mic Mac formation has been interpreted as a likely source rock for the Scotian Basin (Mukhopadhyay and Birk, 1989) but no evidence of this formation was found in the available well data for the study area. Other shale-rich units with source rock potential are the Missisauga and Verrill Canyon formations, or the slightly deeper and older Misane member of the Abenaki Formation. The Verrill Canyon Formation is a seaward, shale-rich equivalent to the Mic Mac and Missisauga Formations, and has been selected as a likely source rock for the study-area. Despite its lower organic content, the deeper and older Misane shale was selected as another potential source rock and a separate simulation was run to test the results of this deeper source rock on maturation. Source rocks were given a conservative TOC value of 5% and a Hydrogen Index (HI) of 500 (Table B.5). Type IIB kerogen is common in the Scotian Basin (Mukhopadhyay and Birk, 1989) and was thus selected as the kerogen type for the source rocks. A small section of the Banquereau_5 layer located directly above the largest most landward diapir (D1, Fig. 3.3) was also assigned as a source rock in both simulations (Misane source and Verrill Canyon source models) in order to test whether or not increased heat-flow above salt diapirs would result in hydrocarbon maturation (Fig. 3.12).

Landward regions of the Missisauga Formation are known to be sand-rich and form good potential reservoir rocks. Although it is known that much of this formation shales out before the slope, some sections of the Missisauga were assigned a more sand-rich facies to include some reservoir rocks in the model. Eight regions of the Missisauga Formation were assigned the sandstone facies, and the locations of these sand bodies can be seen in Figure 3.13. Six of these reservoirs are located along the traces of lines 88-1a and 1400 near salt diapirs, and two larger sand bodies were placed in the unconstrained

central part of the model.

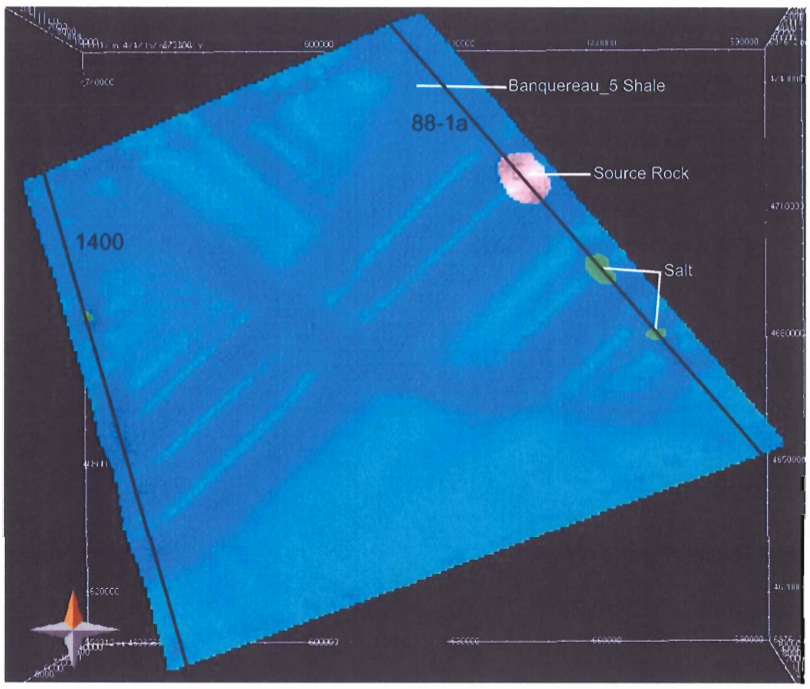

Figure 3.12: *Surface view of Banquereau_5 layer showing location of source rock. The source rock directly overlies the peak of a large salt diapir (D1 in Figure 3.3).*

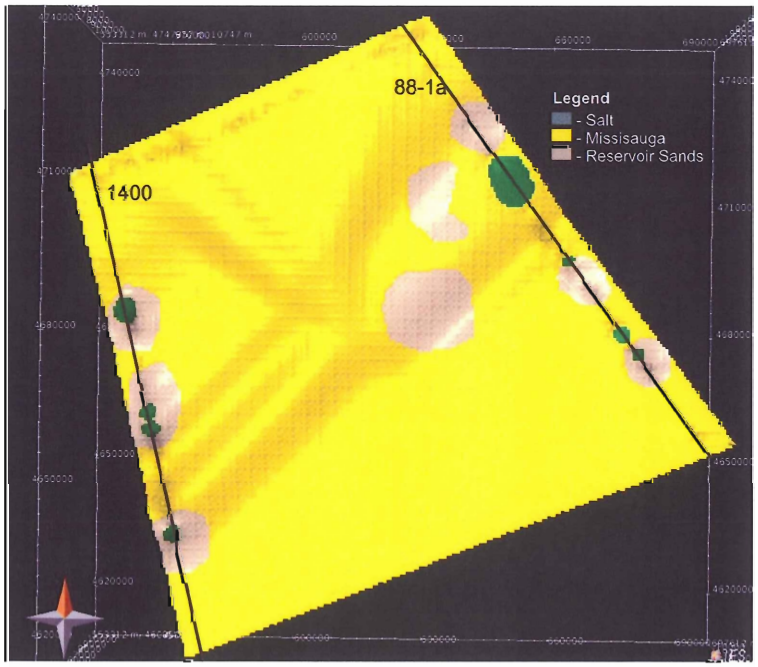

Figure 3.13: *Surface view of the Missisauga Formation showing locations of reservoir rocks and salt diapirs. Locations of lines 88-1a and 1400 shown in black.*

3.3.1 Verrill Canyon source rock results

The simulation for the model with the Verrill Canyon as a source rock showed that the boundary conditions and source rock properties assigned generated hydrocarbons in the Verrill Canyon source rock (Fig. 3.14), but not in the Banquereau_5 source rock. Approximately 6 megatons of liquid hydrocarbons were generated in peak areas, but no vapor hydrocarbons were produced. The hydrocarbons easily migrated from the Verrill Canyon source to the overlying Missisauga reservoirs where oil accumulated but did not saturate the reservoir sands. There were 12 liquid accumulations in total yielding ~82300 MMbbls of oil (Fig. 3.15). *These numbers are strongly dependant on the input data; they should only be considered for comparison and they should not be quoted out of context.*

3.3.2 Misane source rock results

The simulation of the model with the Misane member as the source rock resulted in the generation of hydrocarbons in this source rock (Fig. 3.16), but not in the Banquereau_5 source rock. The Misane generated almost 17 megatons of liquid hydrocarbons, and 2 megatons of vapor hydrocarbons in peak areas. Migration of the hydrocarbons from the Misane source to the Missisauga reservoirs resulted in both oil and gas accumulations. The reservoir sands were not saturated. In total there were 15 oil accumulations and 4 gas accumulations (Fig. 3.15). The model calculated liquid accumulations of ~50400 MMbbls, and vapor accumulations of ~1200 Mm^3 in the reservoirs (Fig. 3.17).

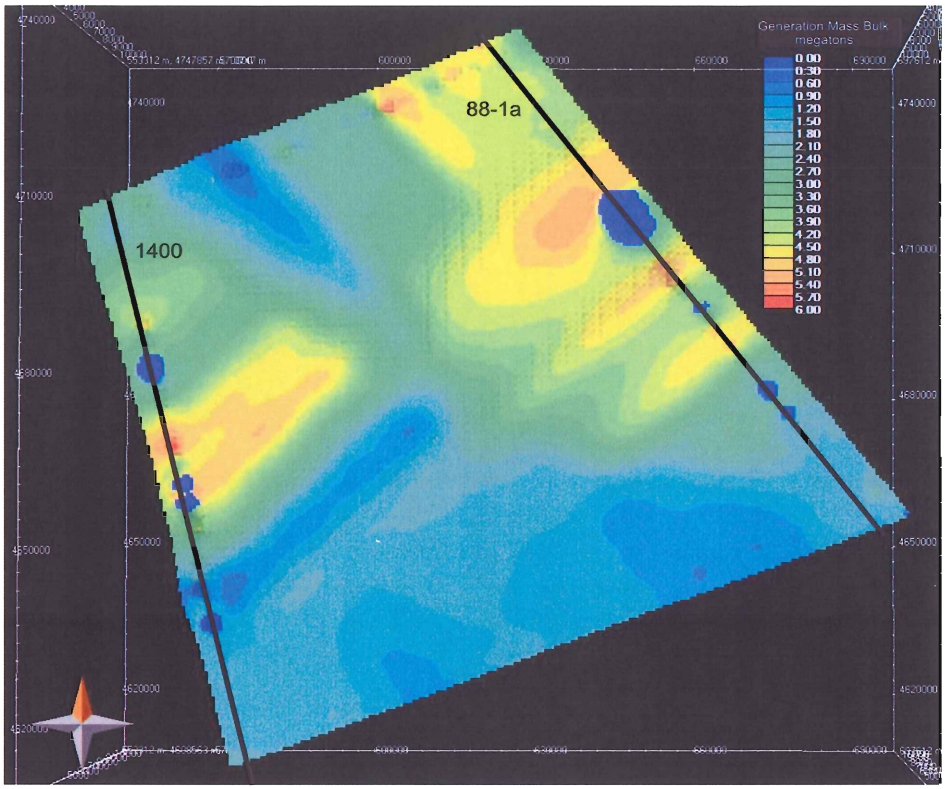

Figure 3.14: *Hydrocarbon generation from the Verrill Canyon source rock (mass bulk).*

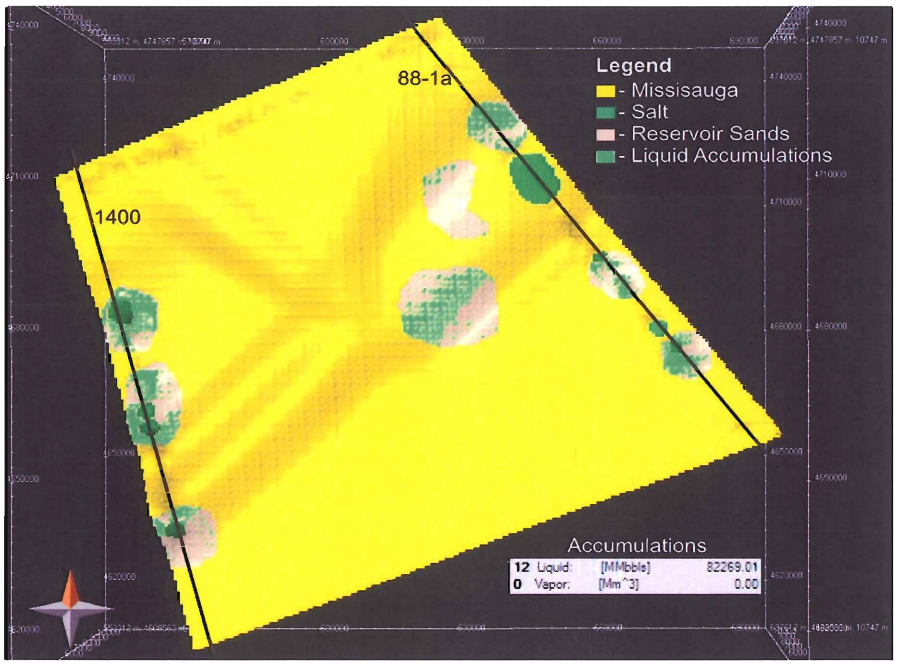

Figure 3.15: *Surface view of the Missisauga Formation showing hydrocarbon accumulations from Verrill Canyon source rock.*

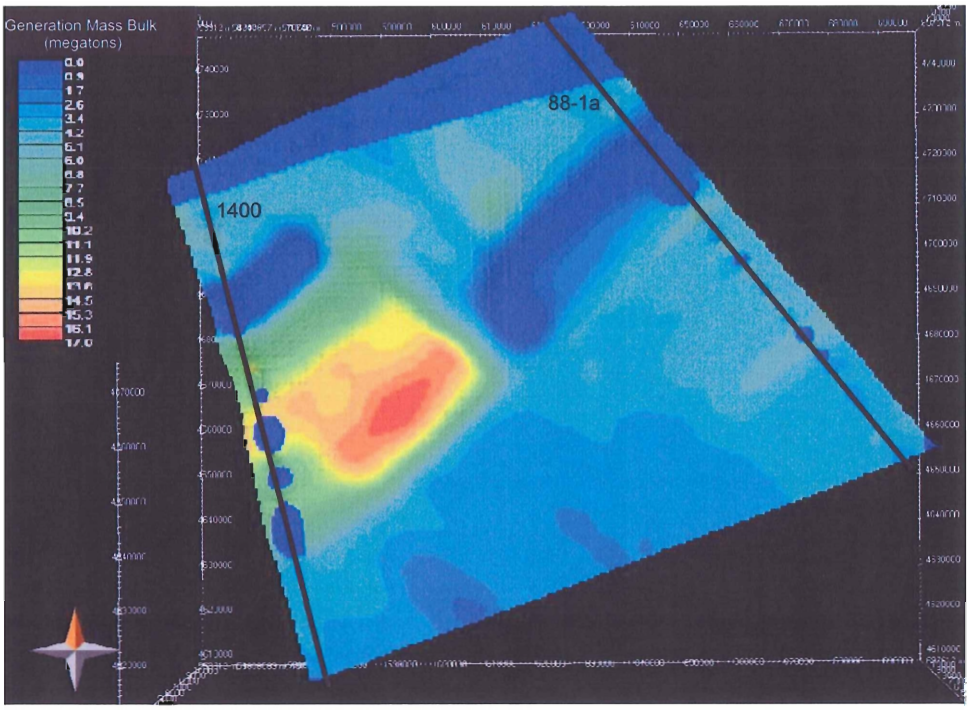

Figure 3.16: *Hydrocarbon generation from Misane source rock (mass bulk).*

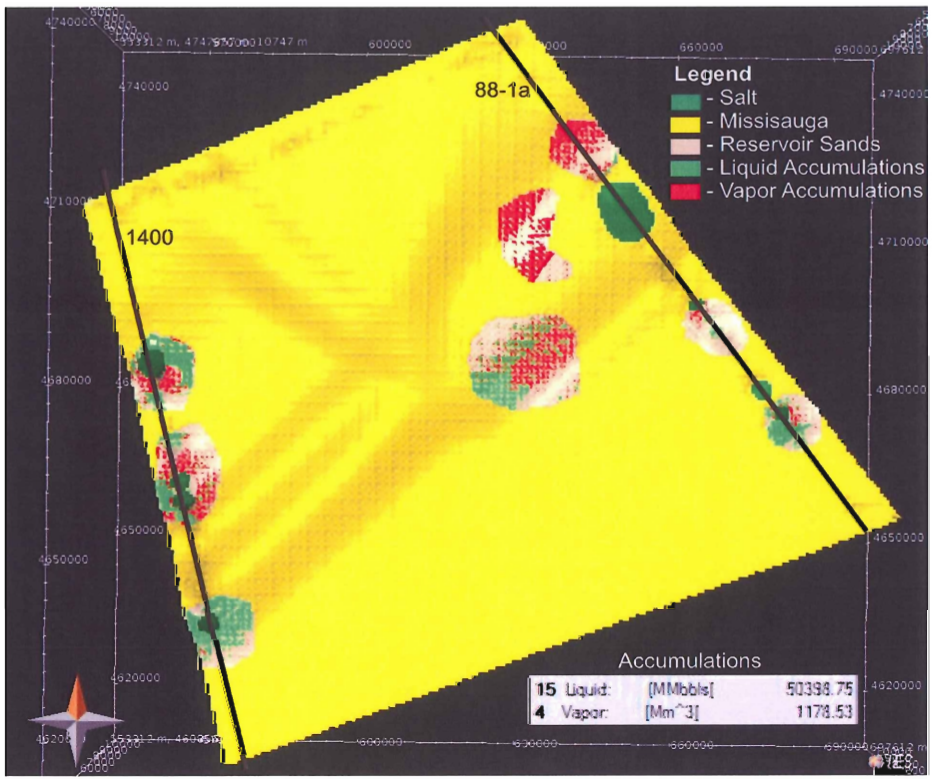

Figure 3.17: *Surface view of the Missisauga Formation showing hydrocarbon accumulations from Misane source rock.*

Chapter Four: Discussion

4.1 Seismic interpretations

The seismic interpretations of lines 88-1a and 1400 show large salt diapirs in the regions of the Scotian Slope studied in this project. Line 88-1a has fewer diapirs than line 1400, but the diapirs in 88-1a are taller, piercing more strata and reaching closer to the surface than those in line 1400. These differences are likely the result of different basement configurations and/or sedimentation patterns between the two lines. As imaging under salt is generally poor, we must look for different methods of interpreting the basement beneath salt to help explain differences in diapir shape. Different salt thicknesses may also play a role in determining the size of the diapirs, as thicker salt means more salt supply feeding into the diapirs as they grow. Further analogue modelling could be used to better determine the effects of sedimentation rates, initial salt thickness and basement configuration on diapir shape.

4.2 Heat-flow

Goutorbe et al. (2007) predicted average heat-flow values in the Scotian Basin of ~36.5 mW/m^2 over basement with ~8.1 km of sediment cover, and ~47.9 mW/m^2 over regions with ~4.6 km of sedimentary cover. The seismic interpretation of the study area indicates an average sedimentary cover of ~6-7 km, thus heat-flow is expected to fit somewhere between these two values at around 41-44 mW/m^2. The average heat-flow calculated by the model for the study area is somewhere between 45 and 50 mW/m^2. These values seem a bit high but are feasible. The predictions made by Goutorbe et al. (2007) are generalized for the entire Scotian Basin, and do not discuss the effect of salt or different crustal configurations on heat-flow, which may explain the higher predicted

heat-flow by the model. The model shows very high surface heat-flow over salt diapirs, reaching ~78 mW/m^2 (Fig. 3.7). The heat-flow increase above the diapirs is confined to the regions directly above the diapirs, dropping to the average basin levels almost immediately in the regions adjacent to the diapirs. This is important when assessing the hydrocarbon potential associated with increased maturation above diapirs as it means that if increased maturation were to occur it would be confined to only the regions directly overlying the diapirs.

The amount of increase in heat-flow above diapirs is directly related to the height of the diapirs. The tallest diapirs are located along line 88-1a. These diapirs reach closer to the surface than those on line 1400, and accordingly, result in higher surface heat-flow values. The width of the diapirs also has an affect on the heat-flow. Wider diapirs are able to absorb more heat due to their larger surface area than smaller diapirs. The edges of large salt diapirs have more contact with surrounding sediments than smaller diapirs, and are thus able to absorb more heat. However, they also have a larger volume over which they must distribute the heat absorbed from these surrounding sediments. Thinner diapirs have a smaller surface area than larger diapirs and absorb less heat, however due to their smaller volume, they are able to reach higher heat-flow values than larger diapirs as the heat isn't distributed over such large volumes (Fig. 3.10).

Heat-flow measurements in July of 2008 will be taken at the most interesting locations based on heat-flow predictions made by the model. Interesting regions for heat-flow measurements would be over the salt diapirs that reach nearest the surface, and with the highest predicted surface heat-flow values: above diapir D1 in line 88-1a at shotpoint 2975 (Fig. 4.1) (has the highest predicted surface heat-flow). Measurements should also

be taken above diapir D2 at shotpoint 3260 and at the landward tip of its associated canopy C1 at shotpoint 3340 (Fig. 4.1) to test the affect of salt canopies on heat-flow. Heat-flow measurement from the seaward limit of study area along line 88-1a at shotpoint 3825 would be useful as it would give us a measure from an area unaffected by salt showing the general heat-flow of the region. Ideally many measurements would be taken from regions unaffected by salt diapirs to find the general trend in heat-flow for the area.

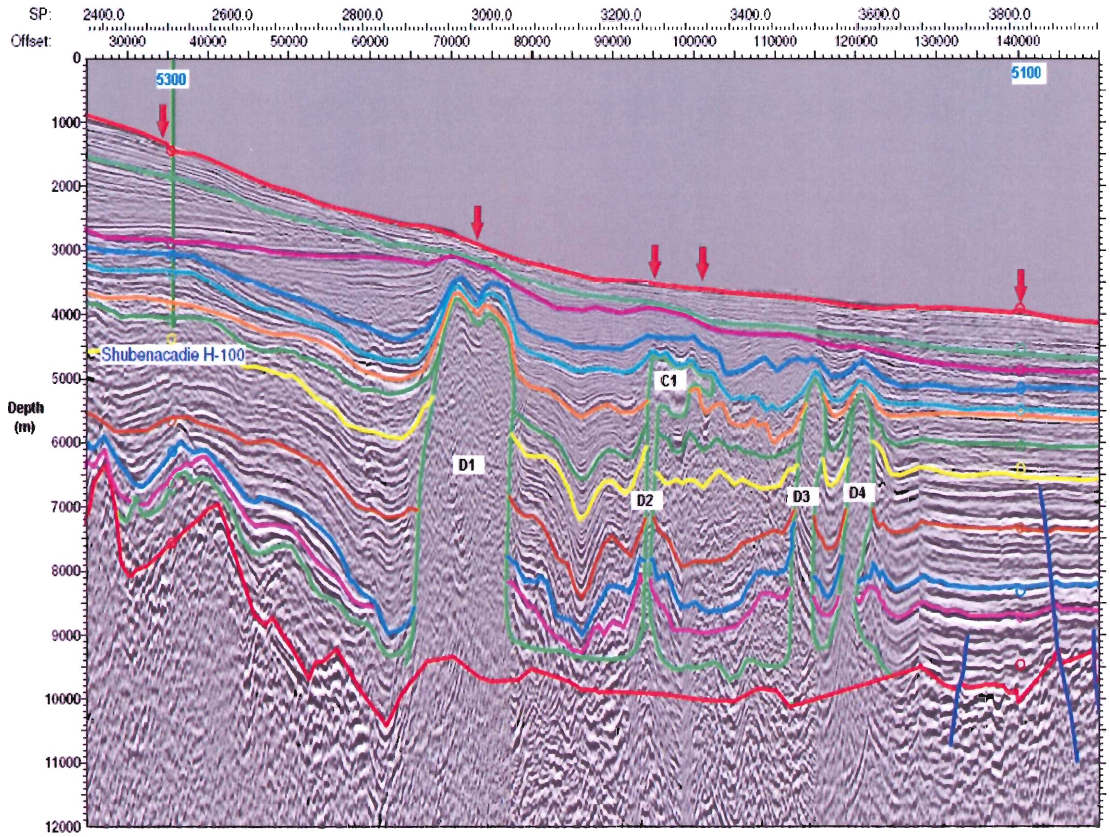

Figure 4.1: *Line 88-1a with red arrows showing locations for future heat-flow measurements.*

Heat-flow measurements above the diapirs in line 1400 at shotpoints 2600 and 1725 (Fig. 4.2) would be useful as they would allow us to test the effects of salt diapirs

on heat-flow at greater depths from the surface. These measures would allow us to evaluate the effect of sediment cover above the diapirs on heat-flow. Measurements should also be taken from each corner of the study area where the seismic lines cross, to observe the general variation in heat-flow throughout the region. These could be taken along line 88-1a at shotpoints 2490 and 3825 (Fig. 4.1), and along line 1400 at shotpoints 3200 and 1165 (Fig. 4.2).

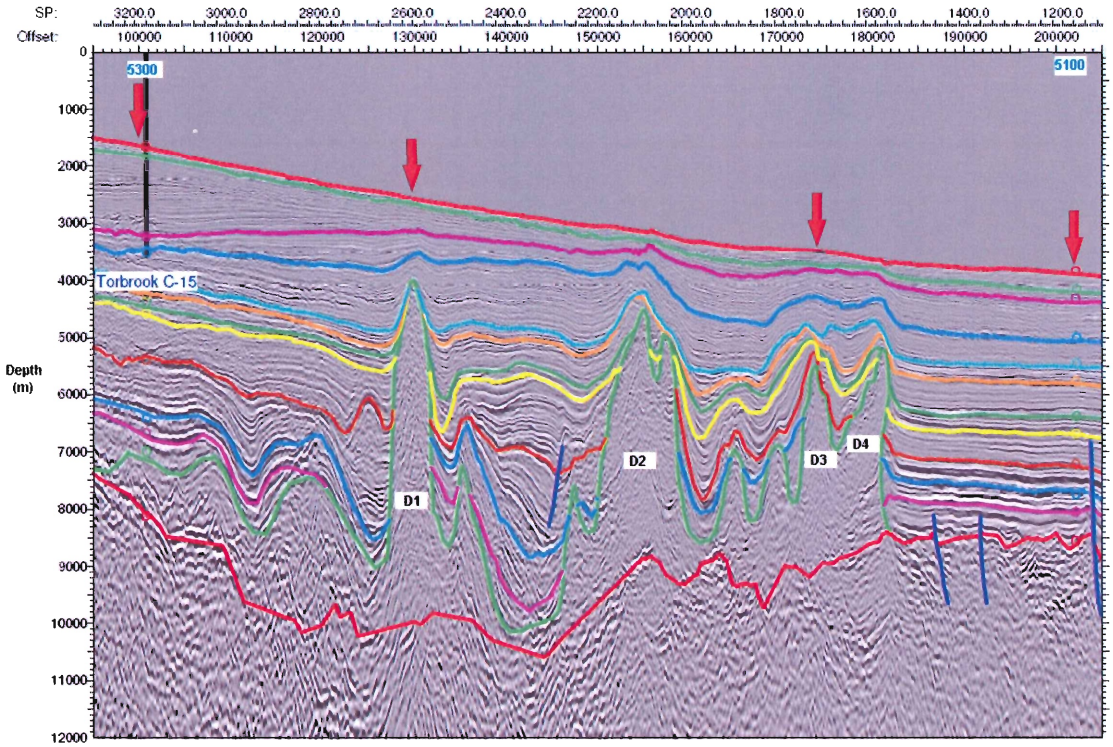

Figure 4.2: *Line 1400 with red arrows showing locations for future heat-flow measurements.*

4.3 Petroleum systems modelling

The petroleum systems modelling portion of this project predicts that with the assigned boundary conditions and lithologies there will be some hydrocarbon generation. It is not to be taken as an accurate account of the petroleum systems in the study area but rather as a theoretical application as to whether petroleum systems are possible and what

further work needs to be done in order to accurately identify petroleum systems in the study area. The numbers produced by the models for hydrocarbons generated and accumulations are highly dependant on the input data. With the lack of wells in the study area, much of the input data has been inferred from the Scotian Shelf to show the potential under assumed circumstances, and thus the results should not be quoted out of context. Two models were run testing the hydrocarbon potential with the Misane Member layer as a source rock and with the Verrill Canyon Formation as a source rock and are discussed below. These will be referred to as models 1 and 2 respectively.

The specified source rock of the Misane shale in model 1 may not form a good source rock in nature, but was selected as a source in order to test the results of having an older source rock located at depth. The Missisauga reservoir rocks may have completely shaled out by the deep water slope regions of the Scotian Basin modeled, but again, for lack of better constrained reservoir rocks the Missisauga Formation reservoirs were included to test the accumulation potential of the area. The input parameters for both models 1 and 2 resulted in the generation and accumulation of hydrocarbons.

4.3.1 Generation and accumulation

Model 1 resulted in the generation of almost 17 megatons of hydrocarbons in peak areas. This includes the generation of both oil and gas. Model 1 resulted in the accumulation of ~50400 MMbbls of oil, and ~1200 Mm^3 of gas. Model 2 resulted in the generation of almost 6 megatons of hydrocarbons in peak areas however it generated only oil with accumulations of ~82300 MMbbls. Neither model generated any hydrocarbons in the Banquereau_5 source rock located above diapir D1 in line 88-1a.

The higher hydrocarbon generation and accumulations in model 1 than in model 2 is likely a result of the greater depth, and more importantly, greater thickness of the Misane source rock compared to the Verrill Canyon source rock. The Misane Member source rock has a maximum thickness of ~1000 m while the Verrill Canyon Formation's maximum thickness is only ~200 m. A thicker layer with the same petroleum systems elements means more organic matter and thus increased potential for generation of a greater volume of hydrocarbons. As depth increases the temperature is higher, and thus there is greater potential for hydrocarbon maturation. Increased age means a longer period in which the organic matter may be cooked, and again, further maturation. This likely explains the presence of gas in Model 1, and not in Model 2. The Verrill Canyon source rock wasn't cooked to the point of generating gas and thus resulted in the generation of only oil while the deeper, older and more mature Misane source rock was able to generate both oil and gas.

In model 1 the source rock is separated from the reservoir rocks by the Baccaro and Verrill Canyon units. The abundance of low porosity shale and limestone in the Baccaro Member and Verrill Canyon Formation likely inhibited the migration of hydrocarbons from source to reservoir, resulting in a limited amount of the generated hydrocarbons reaching the reservoirs. In model 2, the source rock directly underlies the reservoir rocks, and thus finding a route of migration was not a problem.

With the increased heat-flow above salt diapirs, it was expected that there would be some maturation in the source rock placed above diapir D1 in line 88-1a. There were however no hydrocarbons generated from this source rock. This lack of maturation is likely a result of the thin sedimentary cover overlying this diapir. There is little sediment

to insulate above the diapir, and the heat simply flows through the material leaving the sediments with little increase in temperature, an essential element for maturation. The thin cover poorly insulates from the cold seawater above at just over 0° C, while maturation requires temperatures of at least 90° C (Hunt, 1996).

4.3.2 Future models

Future models could be run testing the affects of different input parameters on the petroleum system such as increasing the TOC of the source rock above 5% and trying another kerogen type found to be present in the Scotian Basin such as type IIA, or type III (Mukhopadhyay and Birk, 1989). Placing a sandier, more permeable facies between the source and reservoir rocks in model 1 would also increase the expected accumulations in the reservoirs. Mapping some faults between the source and reservoir rocks would have a similar affect in increasing migration. Faults are common in sediment overlying salt as salt deformation highly deforms overlying sediments and those surrounding diapirs (See Appendix A). This is likely a better solution to the problem of poor migration as faults are more likely in this salt deformed deep water region than porous sediments, but the resolution of the seismic and the scope of this thesis did not allow for the introduction of faults in the modelling process.

It is possible that, if source rocks were present above small diapirs with thicker sedimentary cover than the diapir tested in the models, that maturation may occur in these source rocks as a result of the increased heat-flow associated with the salt. To test this theory, future models could include source rocks above some of the smaller diapirs in line 1400.

Chapter Five: Conclusions

Thermal and petroleum systems models created with PetroMod 10 software test the effect of salt diapirs on heat-flow and the first-order petroleum systems potential of the study area. As expected, significantly increased heat-flow is found above salt diapirs. The proximity of the diapirs to the surface has a direct effect on the seafloor heat-flow. Heat-flow above diapirs reaches upwards of ~78 mW/m^2, while surrounding regions show a average heat-flow of 45-50 mW/m^2. Heat-flow measurements in the summer of 2008 should be taken above the tallest and relatively thinly covered salt diapirs, some smaller and deeper buried salt diapirs, and in diapir-free areas in each corner of the study area and along the traces of seismic lines 1400 and 88-1a to determine the general heat-flow for the area unaffected by salt. These measurements would allow us to test the accuracy of the model, to calibrate the effects the diapir size has on heat-flow, and to determine the regional heat-flow trend of the study area. The experimental heat-flow results will also be used to constrain the thermal parameters for future models more accurately.

The model shows that there is petroleum systems potential for the region, but it is highly dependant on the presence and quality of source rocks and especially reservoir rocks, which must be better constrained before anything can be said confidently on the actual potential of the area.

References

Adam, J., Shimeld, J., Krezsek, C., and Grujic, D., 2006. How sedimentation controls structural evolution and reservoir distribution in salt basins. Nova Scotia's Energy Research and Development Forum, May 24-25, 2006, Antigonish, Canada (on CD).

Avery, M.P., 2004. Vitrinite reflectance (Ro) of dispersed organic matter from Chevron-PEX-Shell Acadia K-62. Geological Survey of Canada Open File #4627.

Brun, J.P., and Mauduit, T., 1998. Growth fault/rollover systems: Birth, growth, and decay. Journal of Geophysical Research, **103:**18119-18136.

Enachescu, M., and Hogg, J., 2005. Exploring for Atlantic Canada's next giant petroleum discovery. CSEG Recorder, **30:** p. 19-30.

Enachescu, M., and Wach, G., 2005. Exploration offshore Nova Scotia: Quo Vadis? Ocean-Resources: p. 23-35.

Geissman, J. and Palmer, A.R., 1999. 1999 Geologic Time Scale. Geological Society of America Website: http://www.geosociety.org/science/timescale/timescl.htm

Goutorbe, B., Loubet, N., Drab, L., and Lucazeau, F., 2007. Heat-flow of the eastern Canadian rifted continental margin revisited. Terra Nova, **19**: 381-386.

Hunt, J.M., 1996. Petroleum geochemistry and geology. W.H. Freeman, New York, p. 743.

Hyndman, R., Keen, C., and King, L., 1975. Geological development of the continental margin of Atlantic Canada. Geoscience Canada, **2:** 26-35.

Jackson, M.P.A., and Talbot, C.J. 1991. A glossary of salt tectonics: The University of Texas at Austin, Bureau of Economic Geology Geological Circular, No. 91-4, p. 44.

Jansa, L.F., and Wade, J.A., 1975. Geology of the continental margin off Nova Scotia and Newfoundland. In: W.J.M. van der Linden, J.A. Wade (eds.): *Offshore geology of Eastern Canada,* Vol. 2, Regional geology: Geological Survey of Canada, Paper 74-30, p. 51-106.

Kidston, A.G., Brown, D.E., Altheim B., and Smith B.M., 2002. Hydrocarbon Potential of the Deep-water Scotian Slope, Canada-Nova Scotia Offshore Petroleum Board, Open Report, p. 111.

Louden, K., 2002. Tectonic evolution of the east coast of Canada. CSEG Recorder, **27**: 37-49.

McKenzie, D., 1978. Some remarks on the development if sedimentary basins. Earth and Planetary Science Letters, **40**: 25-32.

Moir, P., Lake, P., King, S., and Williamson, M., 2007. BASIN Database. Natural Resources Canada Website: http://basin.gsca.nrcan.gc.ca/wells/index_e.php

Mukhopadhyay, P.K., and Birk, D., 1989. Organic facies in the Sable Sub-basin, Scotian Shelf. Geological Survey of Canada, DSS. File No: OSC. 88 - 00308 - (014).

Palmer, A., and Geissman, J., 1999. 1999 Geologic Time Scale. Geological Society of America Website: http://www.geosociety.org/science/timescale/timescl.htm

Rowan, M.G., 2005. Salt tectonics and sedimentation: A structural and sedimentary framework for petroleum systems in salt basins.

Shimeld, J., 2004. A comparison of salt tectonic sub-provinces beneath the Scotian Slope and Laurentian Fan. In: P.J. Post, D.L. Olson, K.T. Lyons, S.L. Palmes, P.F.

Harrison, N.C. Rosen (eds): *Salt Sediment interactions and hydrocarbon prospectivity: Concepts, applications and case studies for the 21st century*, 24th Annual GCSSEPM Foundation Bob F. Perkins Research Conference proceedings, p. 291-306.

Shimeld, J., and Wade, J., 2005. Seismostratigraphic Interpretation of the GX Technology NovaSPAN seismic survey, Nova Scotia Margin, Canada. *GX Technology publications.*

Vendeville, B.C., and Jackson, M.P.A., and., 1992. The rise of diapirs during thin-skinned extension. Marine and Petroleum Geology, **9**: 331-353.

Wade, J.A. and B.C. MacLean., 1990. The geology of the southeastern margin of Canada. *Geology of the Continental Margin of Eastern Canada*. M. J. Keen and G. L. Williams. **2:** p. 167-238.

Wade, J.A, MacLean, B.C. and Williams, G.L. 1995. Mesozoic and Cenozoic stratigraphy , eastern Scotian Shelf. new interpretations. Canadian Journal of Earth Sciences, **32**: 1463-1473.

Wielens, J.B.W., Jauer, C.D., Williams, G.L., 2006. Is there a viable petroleum system in the Carson and Salar Basins, offshore Newfoundland? Journal of Petroleum Geology, **29**: 303-326

Wu, Yue, 2007. Crustal structure of the central Nova Scotia Margin and the transition from volcanic to non-volcanic rifting off Eastern Canada. PhD. thesis, Department of Earth Sciences, Dalhousie University, Halifax, N.S.

Young, J.L., 2005. The stratigraphy and structural history of the Mesozoic and Cenozoic of the central Nova Scotia Slope, Eastern Canada. M.Sc. thesis, Department of Earth Sciences, Memorial University, St. John's, N.F.L.D.

Yu, Z., Lerche, I., and Lowrie, A., 1992. Thermal impact of salt: Simulation of thermal anomalies in the Gulf of Mexico. Pure and Applied Geophysics, **138**:181-192.

Appendix A - Analogue Modelling and Interpretations

Appendix A contains 3 sections:

A-1: General overview of salt tectonics on passive margins

A-2: Model configuration and modelling procedures, and

A-3: Interpretation of analogue model Experiment 5-7

A-1: Introduction to salt tectonics on passive margins

Salt is found to behave as a viscous material and begins to flow under differential loading of overlying sediments (Fig. A.1). In passive margins, sedimentation generally

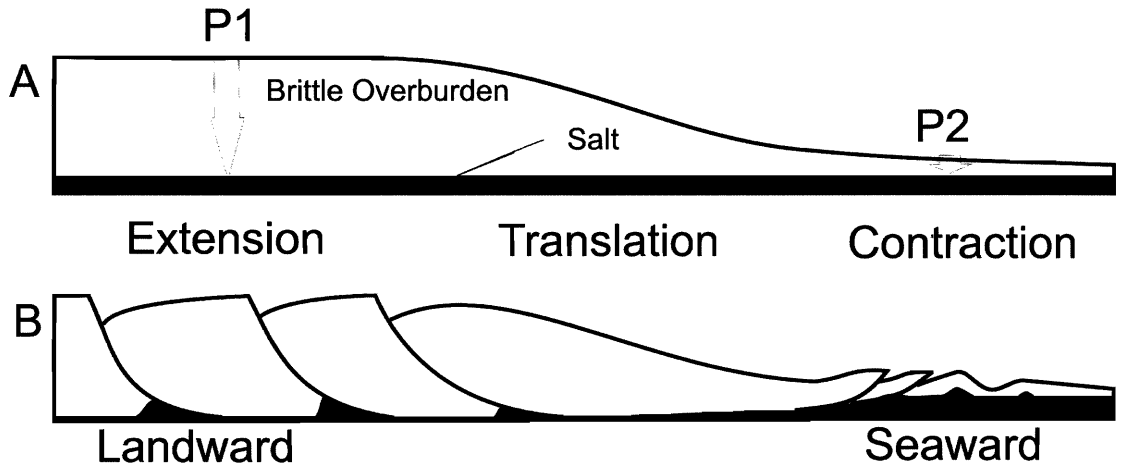

***Figure A.1**: Thin skinned extension in a passive margin setting. A sedimentary wedge on top of a viscous salt substratum. Top figure (A) depicts the differential pressure that initializes salt flow. Bottom figure (B) depicts growth fault rollover systems present in the shelf to slope transitional region and seaward thrusting. (Modified from Adam et al., 2006)*

progrades seaward, as sediment must pass over and fill any landward basins before further seaward advance can occur, thus sedimentary cover thickens landward before seaward. The greater overlying pressure in the landward regions of salt basins causes salt to flow towards seaward regions of lower overpressure, essentially being squeezed out. This causes landward extension as the salt is evacuated, which, if properly balanced, is accommodated by seaward contraction. The evolution of salt withdrawal basins and salt

structures are controlled by sedimentation rates, salt mobilization, and gravity driven deformation (Adam et al. 2006).

Growth fault/rollover systems are common in passive margins. They often occur when brittle sediment overlies a more ductile base such as salt that can form a decollement surface on which gravity driven deformation may occur (Fig. A.1) (Brun and Mauduit, 1998). Concave upwards seaward verging normal faults (listric faults) tend to form as salt is pushed seaward by differential loading from the overlying sediments. Sediments deposited on the hanging wall side of the fault tend to bend downwards into the footwall block as displacement occurs during the fault's growth (Brun and Mauduit, 1998).

Salt diapirs are almost always associated with passive margin salt tectonics. Salt diapirs are vertical to near vertical masses of salt that appear to have intruded the overburden. Salt has a density of 2.2 g/cm^2 that is constant with depth, unlike most sediments which become compacted upon burial thus increasing their density with depth (Young, 2005). In early studies of salt tectonics it was believed that because salt behaved like a viscous fluid, it would flow to the surface due to its lesser density. More recent studies have shown that this is not the case as the overburden, despite its lesser density, behaves as a brittle solid rather than a fluid, and thus prevents the salt from penetrating towards the surface (Vendeville and Jackson, 1992).

Diapirs are formed as a result of extension in the overburden resulting in its stretching and thinning, creating a differential overpressure above the salt. Diapir formation occurs in 3 stages, reactive, active, and passive diapirism (Vendeville and Jackson, 1992). As extension occurs a graben is formed at the surface, and an inverse

graben is formed within the sediments above the salt. It is in this region that there is a lesser overpressure atop the salt than in surrounding areas (Fig. A.2). During the initial reactive stage of diapirism, salt reacts to the space formed by thinning and fills the inverse graben forming a small triangular diapir by movement applied from the differential overpressure (Vendeville and Jackson, 1992). The next stage of diapirism, active diapirism, is the period in which a diapir pierces through the overburden reaching the surface (Fig. A.2). This occurs as a result of further thinning of the overburden by structural or erosional forces to the point where the differential fluid pressure between the salt and the overburden is great enough for the salt to pierce the surface (Vendeville and Jackson, 1992).

The final stage of diapirism is passive diapirism, which refers to the continued growth of a diapir via downbuilding by continued sedimentation once the tip of the diapir has reached the surface (Fig. A.2). The crest of the diapir may be at or just beneath the surface during this final period of growth (Vendeville and Jackson, 1992). The diapir will grow vertically if sedimentation keeps pace with salt extrusion, it will taper in thickness if sedimentation outpaces salt extrusion, and it will spread laterally if sedimentation does not keep pace with salt extrusion (Young, 2005). Diapirs will continue to grow as long as there is sufficient differential overpressure and an abundant salt source.

Salt canopies are structures in which salt is extruded onto the surface as diapir overhangs or sheets, where it coalesces to form one large canopy covering the seafloor (Jackson and Talbot, 1991). Salt canopies can be classified by the type of diapiric structures which form them.

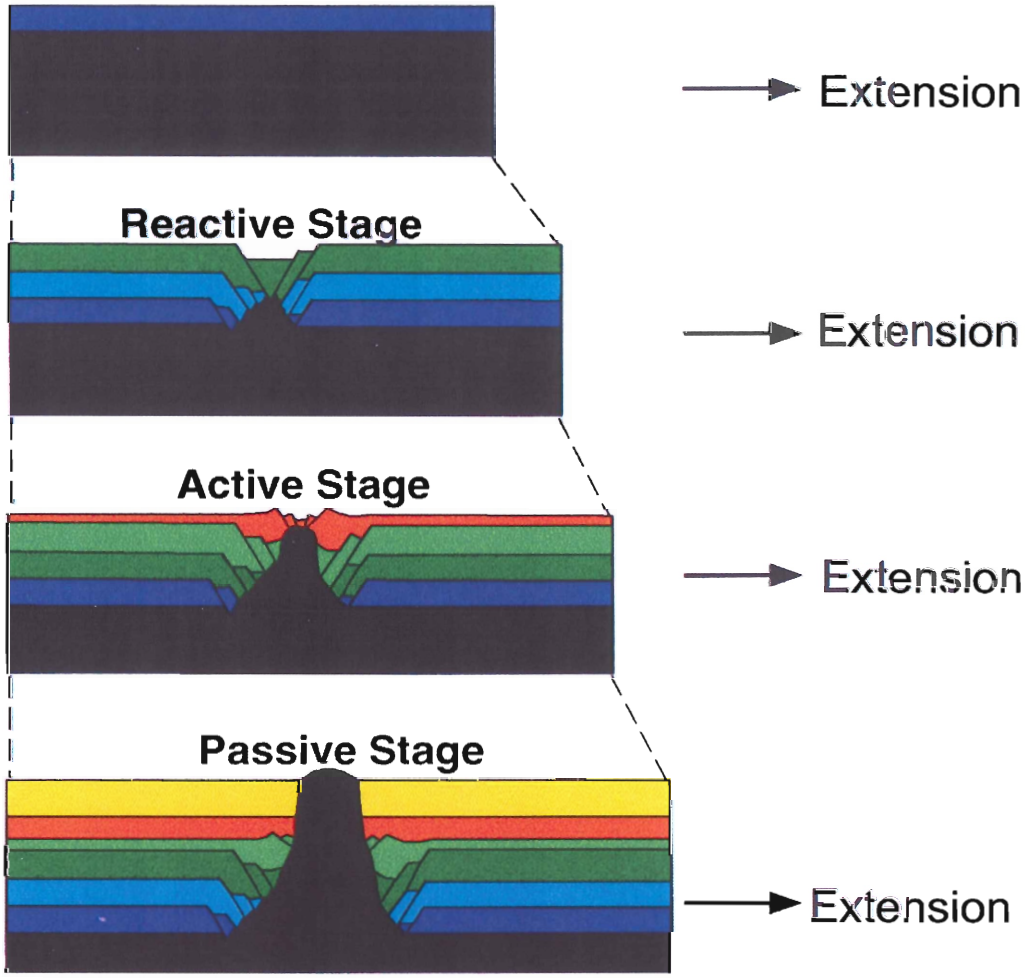

***Figure A.2**: Evolution of a salt diapir (modified from Vendeville and Jackson, 1992)*

Salt stocks are diapirs which are topped with a rounded bulb shaped extrusion of salt, salt tongues are formed from passive diapirs as salt is extruded in a tongue shaped sheet while still attached to the initial feeder located at the landward limit of the tongue (Young, 2005; Jackson and Talbot, 1991).

Salt nappes are similar to salt canopies as they form extensive layers covering sediments supplied by a diapiric feeder, however they are generally far more extensive than canopies, and have only one feeder (Fig. A.3). Salt nappes have a tendency to climb up sediments as they advance while sedimentation continues (Rowan, 2005). Salt nappes

are formed by 3 overlapping processes. The first being depositional loading of deep landward salt sources, the second being basinward translation of the overburden deposited on the initial salt layer, and the third being depositional loading and translation of the oldest most landward regions of the salt nappe (Rowan, 2005).

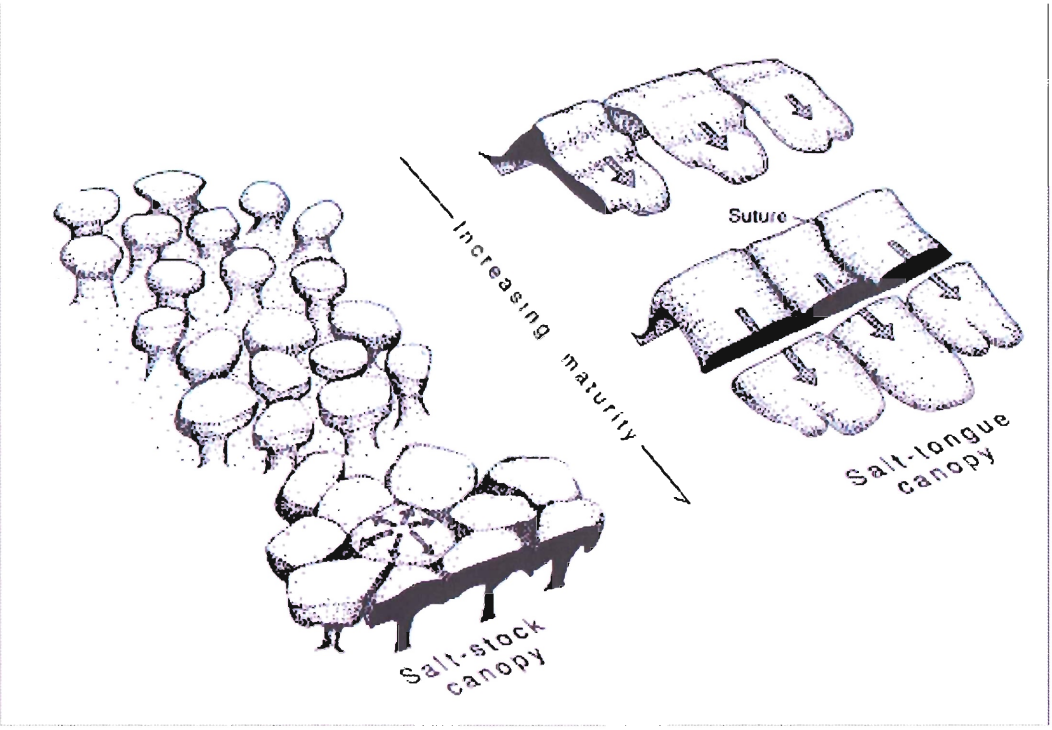

***Figure A.3**: Types of salt canopies (modified from Jackson and Talbot, 1991)*

Salt welds occur where regions once filled with salt become depleted, and overlying strata comes in contact with underlying strata. When this happens in a region of autochthonous salt, it is a primary weld (Rowan, 2005). A weld can also occur in regions of allochtonous salt. Welds may form vertically as diapirs are squeezed closed due to compression, or welds may form in regions of nappes or canopies where salt is evacuated and overlying strata comes in contact with underlying strata. These are examples of secondary welds (Rowan, 2005).

A-2: Model configuration and modelling procedures

Analogue models have proven to be very useful tools in the study of salt tectonics as they provide insight in the evolution of 3D brittle/ductile deformation structures, and provide support for many of the current theories regarding the development of these structures (Vendeville and Jackson, 1992). These dynamically scaled models use sand to simulate sediment, and silicone rubber to simulate salt. The goal of the analogue modelling portion of this thesis is to provide insight into the evolution and timing of salt deformation structures in the Scotian Basin, as well as sedimentary basin evolution in passive margin environments in general.

In this thesis analogue model Experiment 5-7 is interpreted. The model was created in the summer of 2006 by the Dalhousie Salt Dynamics Group. The model was dynamically scaled to represent nature, taking into account materials, scaling for both geometry and time, and basement configuration.

A-2.1 Materials

In Experiment 5-7 silica sand is used to simulate sediment and silicone rubber simulates salt. These materials have been selected based on their physical properties in order to proportionately model the sediments of the Scotian Basin they are representing (Table A.1).

Property	Silica Sand	Silicone Rubber
Grain Size	0.02-0.45	-
Density (g/cm^3)	1.6	0.99
Viscosity (Pas)	-	6*10^4

Table A.1: *Material properties of silica sand and silicone rubber used in analogue model Experiment 5-7.*

A-2.2: Scaling

Analogue model Experiment 5-7 has been dynamically scaled to represent a 70 km wide region of the Scotian Basin with a 2 km deep salt filled full graben basement architecture. The model has been scaled to account for both geometry and time, where 1 cm and 1 hour in the model represent 1 km and 300000 years in nature respectively (Table A.2). The model ran for 196 hours, representing 58.8 Ma of geological time. This model represents the evolution of the Scotian Basin from the Early Jurassic to the Early Cretaceous. The scaling factor for the geometric relationships between model and nature is based primarily on similarities in density and cohesion in sand and sedimentary rocks, while the time scaling factor is based on the viscosity of the silicone, as well as the density ratios of the overburden sand and sediments.

Scaling Parameters	Experiment	Nature
Time	1 hr	300 000 yrs
Geometry	1 cm	1 km

Table A.2: *Scaling parameters showing geometric and time relationships between models and nature.*

A-2.3: Model configuration and setup

Analogue model Experiment 5-7 was created in order to simulate the evolution of salt deformation structures formed by sedimentation atop thick salt filling a rifted full graben basement low (Fig. A.4). Experiment 5-7 was created on a horizontal base which measures 120 cm x 90 cm. The actual experiment is only 70 cm wide, with a 2 cm syn-rift salt basin (Fig. A.5). The extra space on the sides of the experiment allowed for sediment barriers to be built to contain the sieved sediment from spilling over the edges of the experiment.

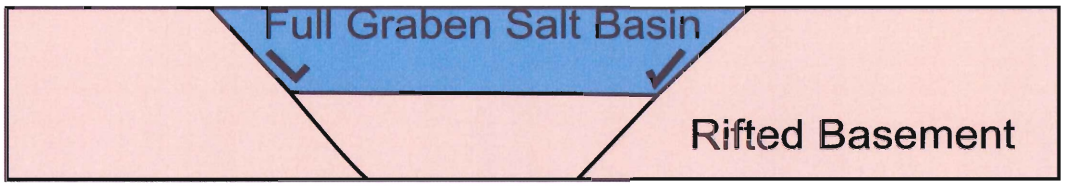

Figure A.4: *Cross sectional view of initial basement configuration for Experiment 5-7.*

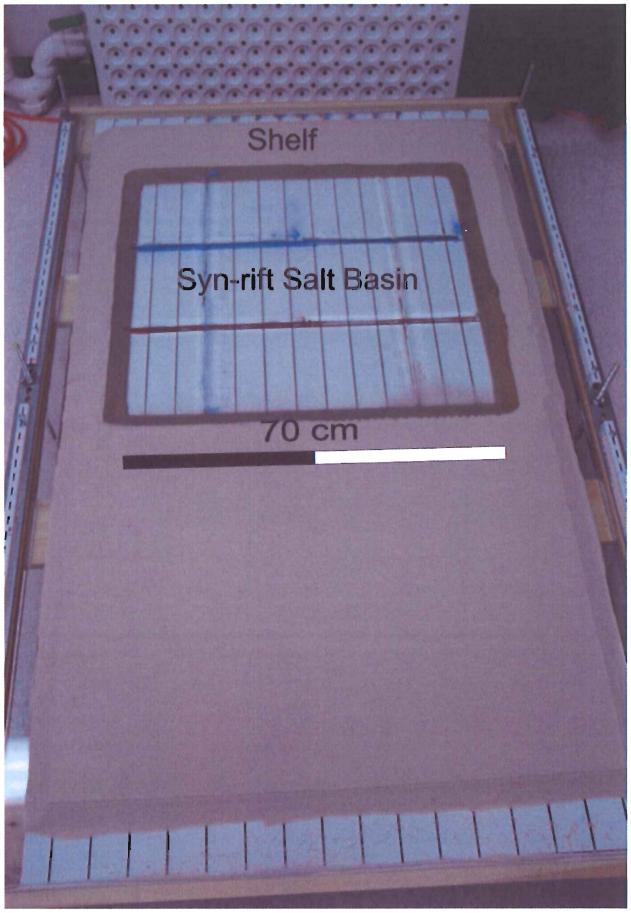

Figure A.5: *Overview of initial configuration for Experiment 5-7.*

A-2.4: Modelling procedures

During modelling, sand was sieved onto the experiment at regular four hour intervals. Each sieve consisted of 700 g of sand being deposited as 2.5 mm thick layers. The mass of sand sieved was calculated and scaled from drill core information from the

Scotian basin, as well as the sand's density, and the thickness and area on which the sand is being deposited. Sand is sieved in a prograding manner, landward to seaward, in order to mimic the natural sedimentation processes of the Scotian Basin. Sieving of sediment is done as quickly as possible in a span of less than 10 minutes. Sediment is sieved to fill all landward lows before advancing seaward. Every fifth layer of sediment is a marker horizon. These marker horizons alternate from red to black in color, and one is deposited every 20 hours representing 6 Ma of geological time. In total there are nine marker horizons. These horizons are important as they are used during interpretation of the finished experiment, as well as in the creation of structural restorations. A detailed account of the timing and colors of sieved horizons can be found in Table A.3. Monitoring of the experiment was done with the use of PIV (Particle Imaging Velocimetry), which allows for detailed interpretations of the model as images are taken every 6 minutes for the entire duration of the experiment.

A-2.5: Sectioning of the model

Once complete, the experiment was cut into sections every 5 cm, with sections running from shelf to slope (Fig. A.6). Prior to sectioning the model is sprayed with water to prevent the sand and silicone from further movement. High resolution digital cameras are used to photograph each section of the model. These images are used to create structural interpretations and structural restorations of the experiment.

Sieving	Color	Interpreted horizon	Time (hours)	PIV#	PIV bS	PIV pS	End sedimentation
0	1st Red		0	1		1	30 cm
1	Green		4	25	241	251	40 cm
2	Blue		8	49	481	494	40 cm
3	Green		12	73	721	733	40 cm
4	Blue		16	97	961	967	30 cm
5	Black	Turquoise	20	121	1201	1209	50 cm
6	Green		24	145	1441	1449	50 cm
7	Blue		28	169	1681	1689	50 cm
8	Green		32	193	1921	1929	50 cm
9	Blue		36	217	2161	2169	50 cm
10	2nd Red	Red	40	241	2401	2410	50 cm
11	Green		44	265	2641	2647	50 cm
12	Blue		48	289	2881	2888	50 cm
13	Green		52	313	3121	3131	50 cm
14	Blue		56	337	3361	3370	60 cm
15	Black	Orange	60	361	3601	3609	60 cm
16	Green		64	385	3841	3849	60 cm
17	Blue		68	409	4081	4087	50 cm
18	Green		72	433	4321	4330	60 cm
19	Blue		76	457	4561	4569	60 cm
20	3rd Red	Green	80	481	4801	4811	60 cm
21	Green		84	505	5041	5048	60 cm
22	Blue		88	529	5281	5290	65 cm
23	Green		92	553	5521	5526	70 cm
24	Blue		96	577	5761	5768	70 cm
25	Black	Brown	100	601	6001	6013	70 cm
26	Green		104	625	6241	6248	70 cm
27	Blue		108	649	6481	missed	missed
28	Green		112	673	6721	6727	75 cm
29	Blue		116	697			70 cm
30	4th Red	Yellow	120	721	7201	11 (use 72	70 cm
31	Green		124	745	7441	7448	75 cm
32	Blue		128	769	7681	7690	80 cm
33	Green		132	793	7921	7928	80 cm
34	Blue		136	817	8161	8169	85 cm
35	Black	Blue	140	841	8401	8411	85 cm
36	Green		144	865	8641	8648	90 cm
37	Blue		148	889	8881	8889	90 cm
38	Green		152	913	9121	9129	90 cm
39	Blue		156	937	9361	9369	90cm
40	5th Red	Violet	160	961	9601	9608	90 cm
41	Green		164	985	9841	9847	95 cm
42	Blue		168	1009	10081	10087	95 cm
43	Green		172	1033	10321	10329	100 cm
44	Blue		176	1057	10561	10567	100 cm
45	Black	Pink	180	1081	10801	10809	110 cm
46	Green		184	1105	11041	11048	110 cm
47	Blue		188	1129	11281	11287	115 cm
48	Green		192	1153	11521	11528	120 cm

Table A.3: *Sieve data for Experiment 5-7.*

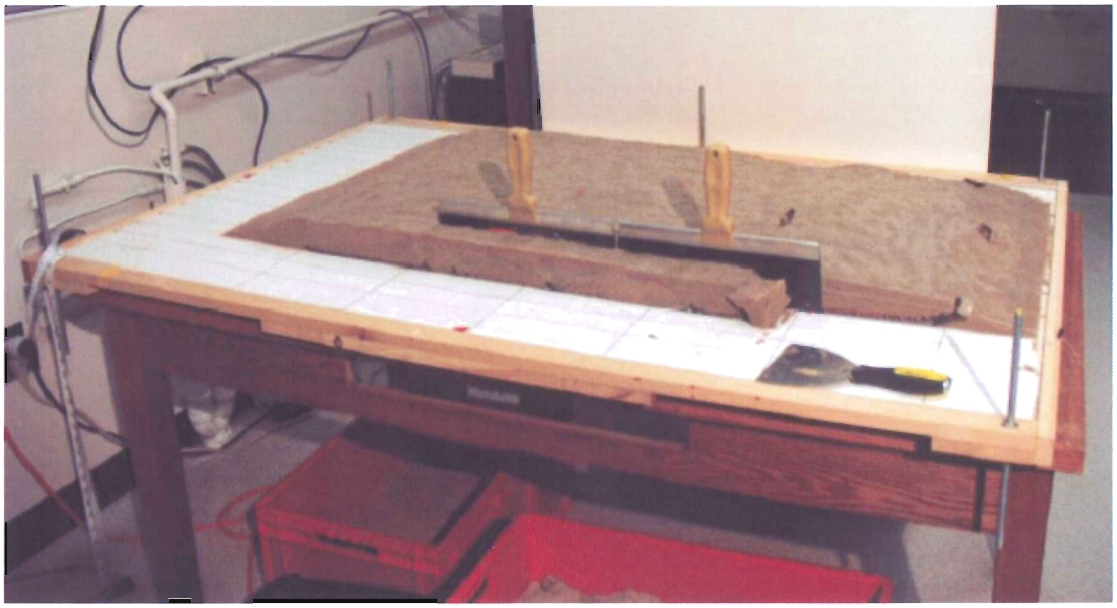

Figure A.6: *Sectioning of an analogue modelling experiment.*

A-3: Interpretation of analogue model Experiment 5-7

Structural interpretations of analogue model Experiment 5-7 in its completed form outlining all salt deformation structures were made in order to determine possible structures associated with prograding sedimentation atop a thick full graben salt basin. A structural restoration was done for one section of the experiment (25 cm section) in order to demonstrate the possible evolution of these salt structures through time. The structural interpretations and restorations of Experiment 5-7 were done in the summer of 2007 with my colleague Matthew Kliffer as part of a Shell SELF summer learning fund work term at Dalhousie University.

A-3.1: Methods of interpretation

The structural interpretations of the model were done by creating a poster showing interpreted cross sections of the model every 5 cm (Fig. A.7). The cross

Experiment 5-7

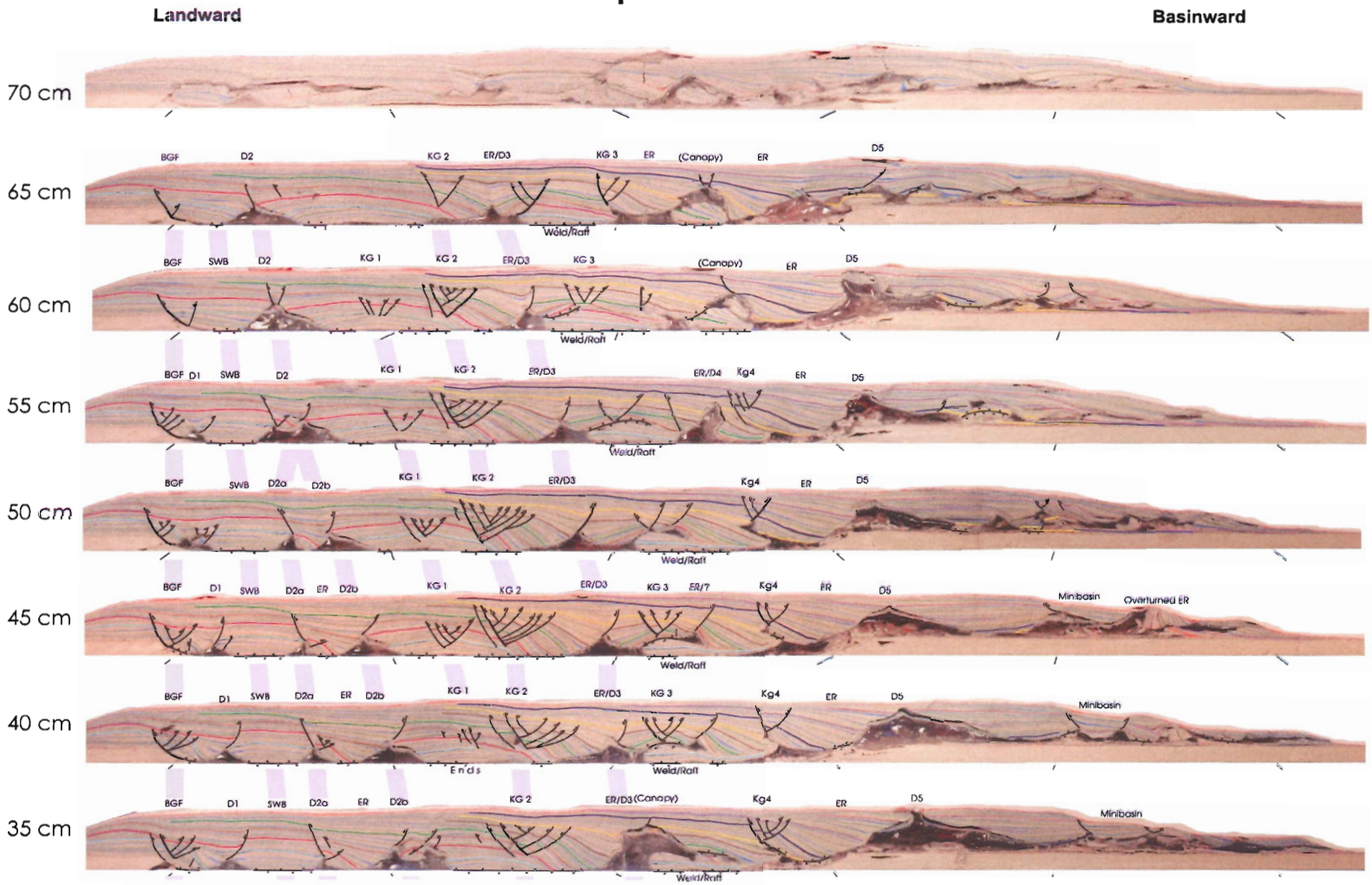

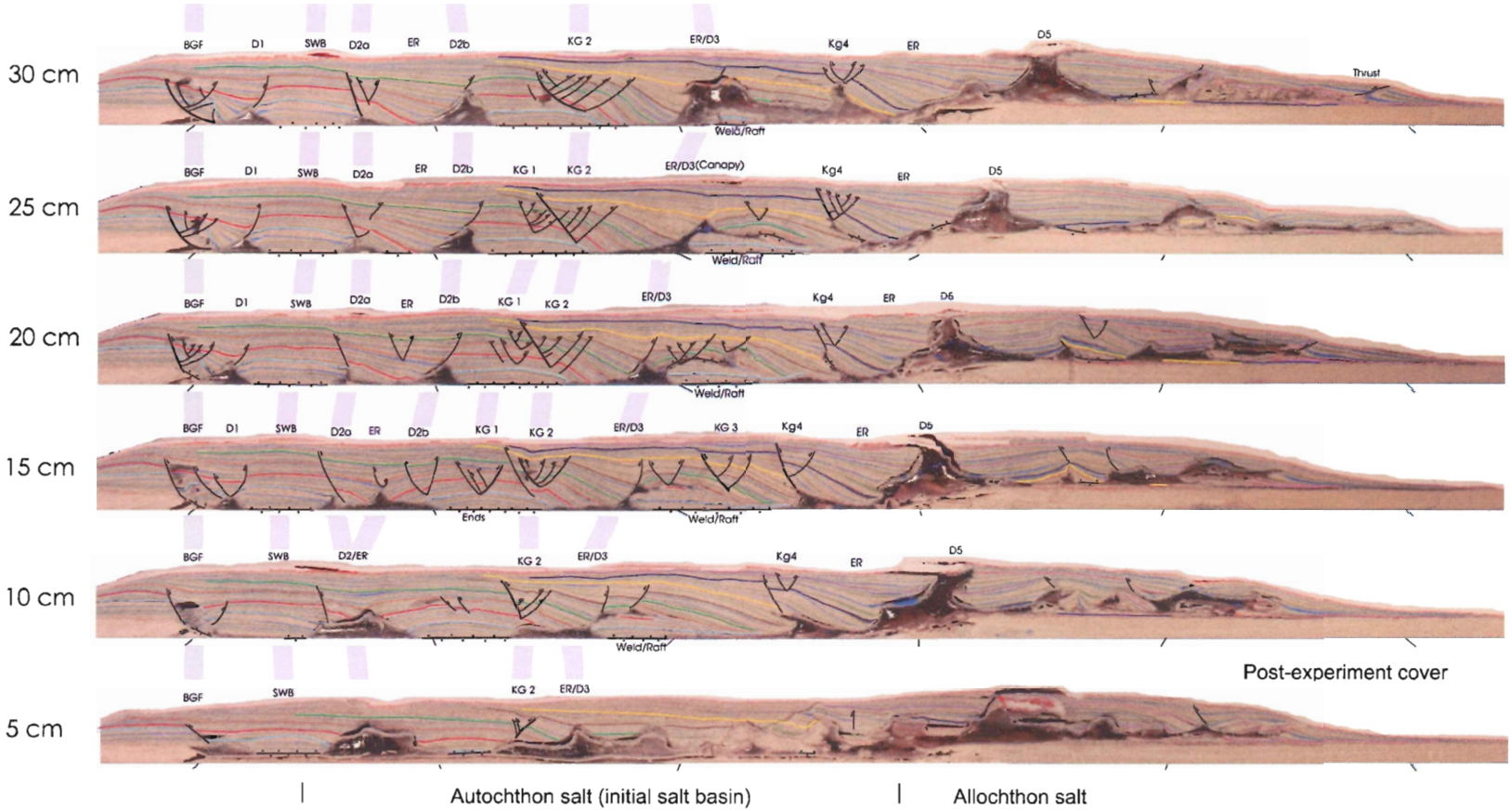

Experiment parameters
Experiment base: horizontal, 70 cm (width) x120 cm (length)
Initial salt ("silicone") basin = 65 cm (width) x 60 cm (length) x 2 cm (thickness)
Sedimentation: constant volume (750 cm^3), sedimentation rate 0.4 mm/yr
Sieving: every 4 hours, max. 0.25 cm thick layers
Duration of experiment = 216 hours

10 cm

Scaling: 1 cm = 1 km

***Figure A.7**: Poster of Experiment 5-7 showing interpretations of salt deformation strucures*

sections were obtained as pictures of each section of the model taken at 5 cm intervals during the sectioning of the experiment. Corel Draw 13 software was used to compile the cross sections in an ordered fashion to make interpretations of salt deformation structures easier. These structures were also interpreted using Corel Draw 13 software. All marker horizons were outlined in brighter colors in order to facilitate interpretations (Table A.3). Faults and welds were then added to the cross sections in black and then finally all structures in the model were labeled and correlated from section to section where possible.

A structural restoration of the cross section at 25 cm was created in order to gain insight into the evolution of structures in the experiment (Fig. A.8). The experiment was restored in stages coinciding to the deposition of the marker horizons, and thus shows the evolution of the model in stages of 20 hours, or 6 Ma in nature. The restorations were done by removing sediment in 20 hour packages from the most recent sediment packages down through the experiment until only the basement and initial silicone were left. Restorations were done by essentially going backwards through the sieving process and removing sediment rather than adding it, returning structures to their original non-deformed state. During restorations, cross section area of both sediment and silicone were kept constant in order to avoid distortions. Marker horizon lengths were also kept constant.

A-3.2: Interpretation of salt deformation structures

Numerous salt deformation structures were identified in Experiment 5-7 (Fig. A.7). These structures include varying types of fault systems and salt bodies. Salt and fault structures are generally related to one another as the whole system evolves

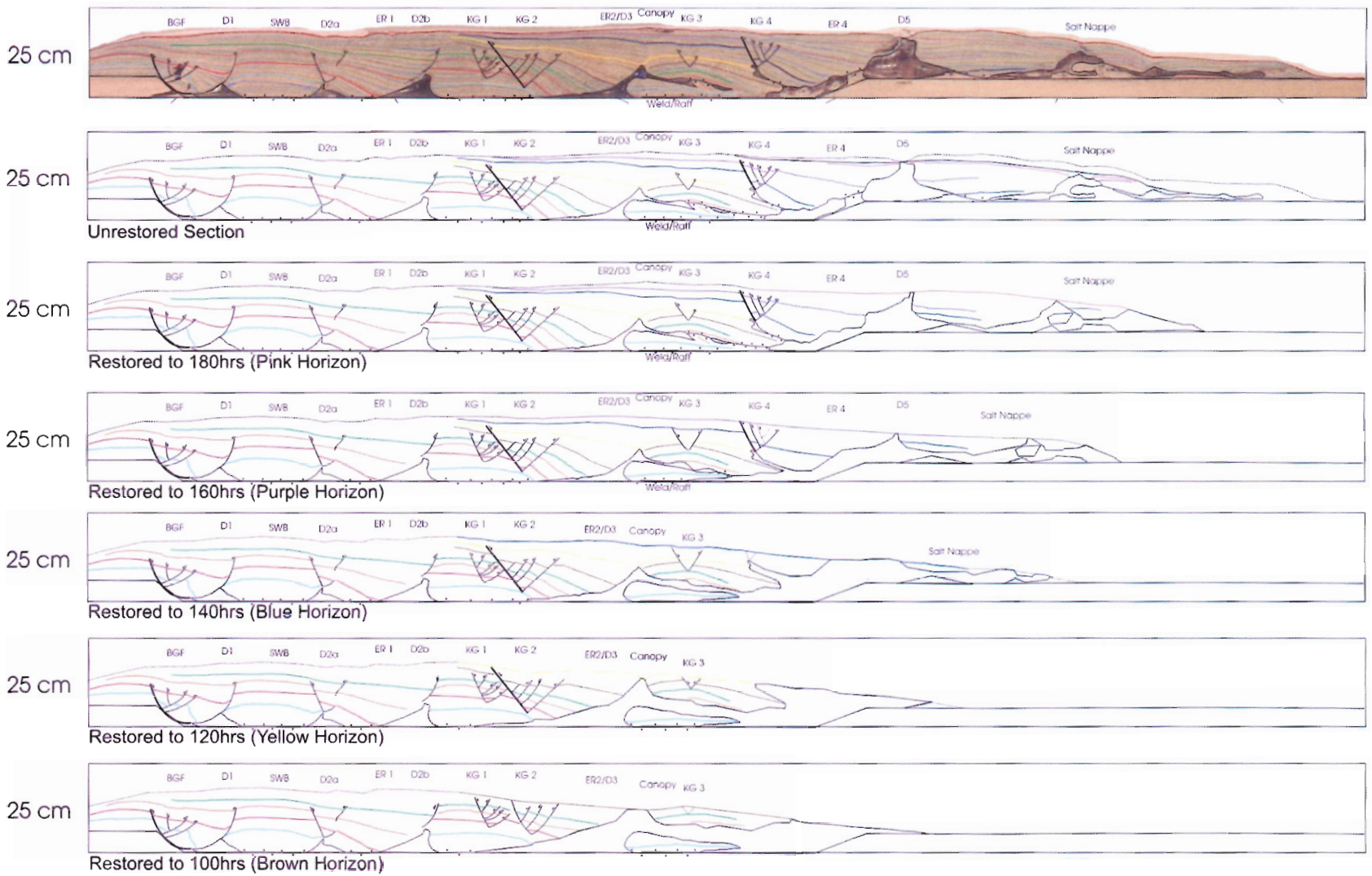
25 cm
BGF
D1
SWB
D2a
ER 1
D2b
KG 1
KG 2
ER2/D3
Canopy
KG 3
KG 4
ER 4
D5
Salt Nappe
Weld/Raft
25 cm
Unrestored Section
25 cm
Restored to 180hrs (Pink Horizon)
25 cm
Restored to 160hrs (Purple Horizon)
25 cm
Restored to 140hrs (Blue Horizon)
25 cm
Restored to 120hrs (Yellow Horizon)
25 cm
Restored to 100hrs (Brown Horizon)

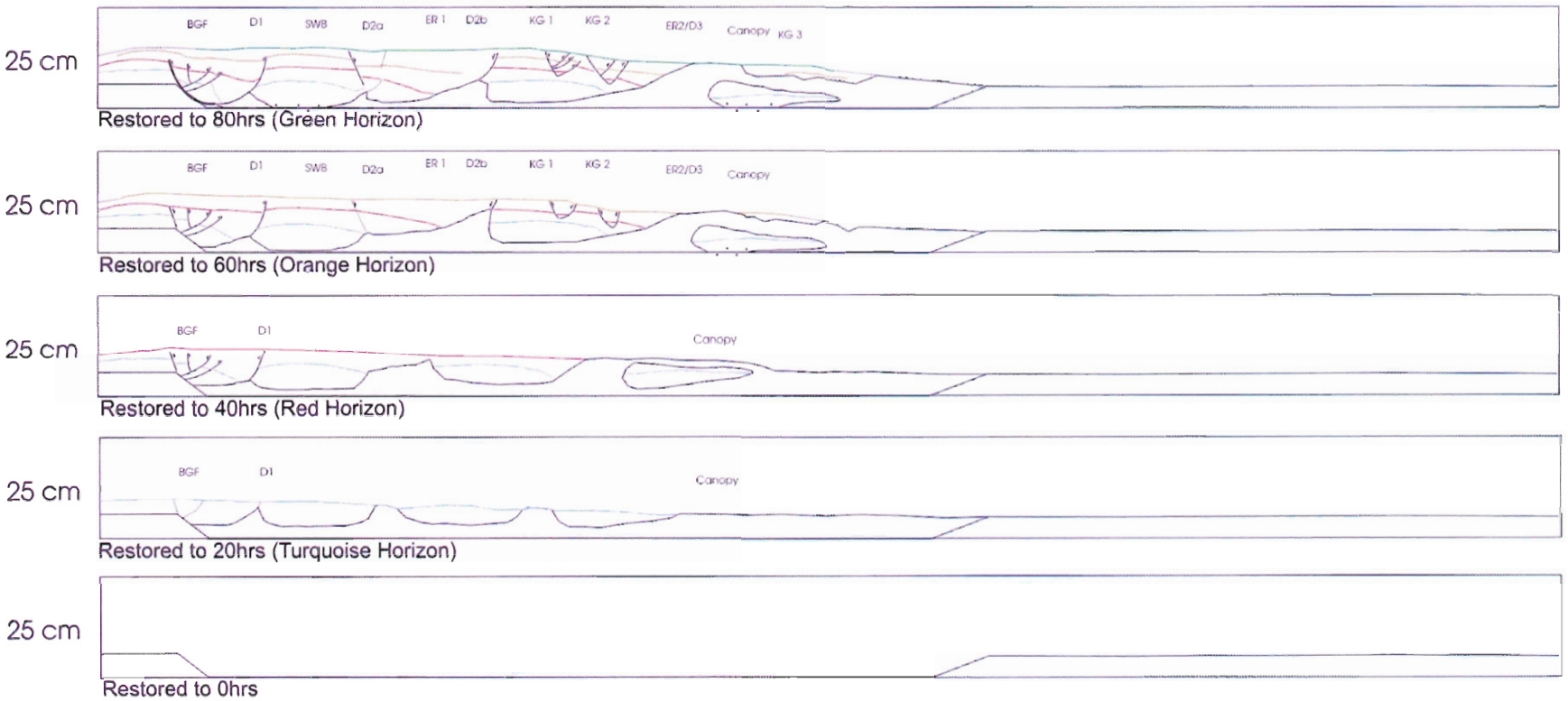

Figure A.8: *structural restoration of Experiment 5-7 (25 cm cross section).*

together. Prominent structures include:

Reactive Diapirs (D): Reactive diapirs were common to almost all sections of the model (Fig. A.9). These diapirs formed in regions where extension and thinning of the overburden allow for intrusion of the salt into the regions of lesser overpressures. The diapirs are generally small and pierce no more than 25 Ma of strata.

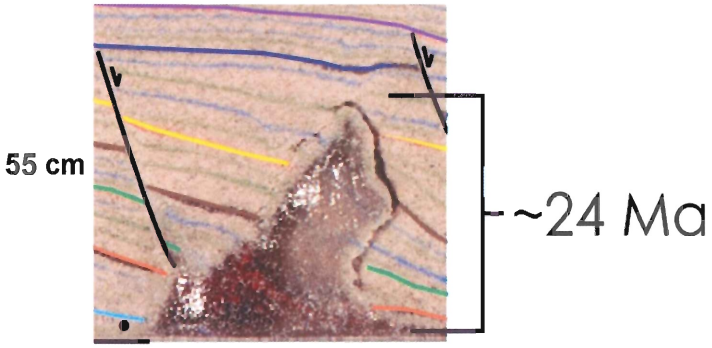

Figure A.9: *Reactive diapir piercing ~24 Ma of strata.* (55 cm in Fig. A.7)

Salt Canopies: One dominant salt canopy was identified in the model (Fig. A.10). This canopy was laterally continuous throughout most of the experiment, forming as a diapir pierced the surface of the model expelling salt laterally seaward atop the experiment surface. The canopy continued to grow for as long as salt supply and diapir growth outpaced sedimentation. This allowed for the excess salt to spread laterally onto the surface. The canopy varies in size laterally and reaches a maximum scaled length of ~70 km.

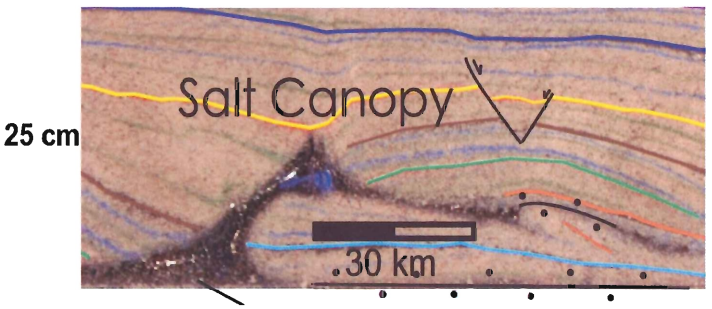

Figure A.10: *Salt canopy in Experiment 5-7. (25 cm in Fig. A.7)*

Basinward Listric Growth Faults (BGF): A basinward listric growth fault has been identified as a laterally continuous structure located at the landward limit of the original salt basin (Fig. A.11). It is present in every section of the model (Fig. A.7). These structures formed as differential loading caused by seaward prograding sedimentation expelled landward salt seaward. Extension was accommodated by the BGF which shows downbuilding sediment packages thickening into the fault.

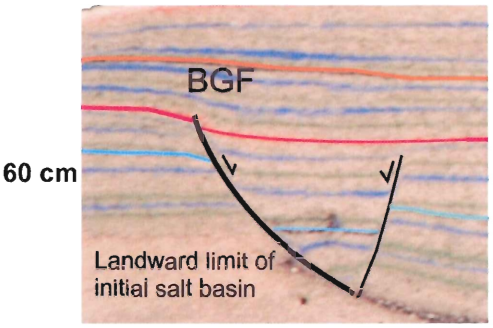

Figure A.11: *Basinward listric growth fault (BGF) located at the landward limit of the initial salt basin. (60 cm in Fig. A.7)*

Keystone Grabens (KG): Multiple keystone grabens have been identified in Experiment 5-7 (Fig. A.12). These small scale extensional structures form in order to compensate for the bending of strata in the crest of rollovers. The keystone grabens identified are almost entirely associated with compensating for rollovers.

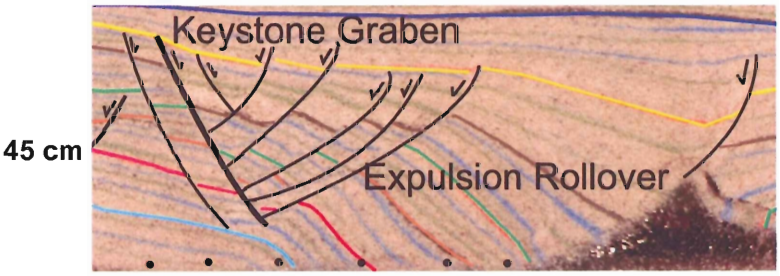

Figure A.12: *Keystone graben accommodating extension in the crest of an expulsion rollover. (45 cm in Fig. A.7)*

Expulsion Rollovers (ER): Expulsion rollovers are found in many sections of the experiment. These structures involve the thickening of sediment associated with the lateral movement of salt in which extension is accommodated by the growth of an adjacent diapir rather than the actual rollover (Fig. A.12).

Salt Withdrawal Basins (SWB): These structures were not common in the model, however one large salt withdrawal basin representing a scaled distance of ~15 km was identified (Fig. A.13). This SWB is laterally continuous and can be correlated across every section of the experiment (Fig. A.7). The basin formed as salt was evacuated laterally resulting from differential loading. As salt was evacuated, regional lows formed in the areas previously filled by salt allowing for accumulation of sediment. As sediment accumulated, the basin continued to grow as more salt was squeezed out laterally. If salt withdrawal and sediment accumulation in the basin is continuous, all the salt will eventually be evacuated resulting in a weld at the bottom of the basin (Fig. A.13).

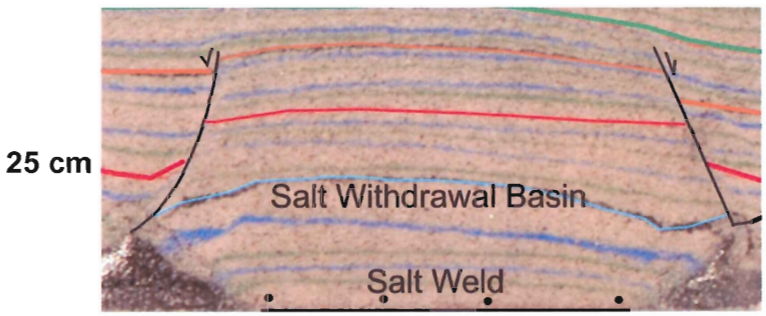

Figure A.13: *Salt withdrawal basin located between two diapirs. Salt has been completely evacuated from this basin forming a weld at its base. (25 cm in Fig. A.7)*

Salt Welds: Salt welds are found both along the basement of the experiment as well as in regions of squeezed canopies where salt is evacuated and the overlying sediment comes in contact with the underlying sediment (Fig. A.13).

A-3.3: Interpretation of structural restorations

A structural restoration was done for the cross section of the model taken at 25 cm (Fig. A.8). The interpretation of the restoration was focused on the timing and extent of diapir growth with respect to sedimentation, and the effects salt supply and sedimentation have on the diapiric structures.

By 20 hours (6 Ma), diapirs D1, D2 and D3 have already begun to form and thus we know that salt movement began almost immediately following the onset of sedimentation. A small listric basinward growth fault (BGF) has begun to form at the landward limit of the salt basin to accommodate the extension associated with the downward movement of sediment as the underlying salt is expelled seaward.

By 60 hours (18 Ma), D1 has become relatively well developed and its growth had begun to slow as a result of a depleting salt source. At this stage, D2 continued to grow as landward sedimentation expelled salt vertically in regions of lesser overpressures, forming the diapir. Sedimentation atop the broad diapir resulted in the formation of two normal faults, one at either edge of the diapir, which accommodated for sediment sinking into the top of the diapir. The diapir was split into two smaller diapirs at this point as sedimentation expelled salt laterally, resulting in an expulsion rollover (ER1). Sediment rolled into D2b to accommodate the extension associated with the salt movement. At this stage, D3 is beginning to form a canopy as salt is expelled seaward onto the sediment surface.

By 100 hours (30 Ma), growth of diapirs D1, D2a and D2b has stopped. The landward salt source for the diapirs has been depleted and sedimentation has advanced seaward beyond the diapirs. This demonstrates that diapir growth occurred early in the system, and lasted only as long as there was sufficient salt supply and a differential sedimentary load to fuel the growth. D3 has formed a large canopy by this point as salt from the diapir reached the surface and spread laterally. An expulsion rollover can be seen flanking the landward edge of the diapir as originally horizontal beds were bent downwards as the underlying salt is expelled during the growth of the diapir. Two

distinct keystone grabens (KG1 and KG2) formed to accommodate the extension in the rolling strata.

By 140 hours (42 Ma), sedimentation had prograded seaward, starting just past diapir D2b. As much of the salt has already been expelled seaward and no more sedimentation occurs in the regions landward of diapir D2b there is no further deformation to these landward regions of the model. Much of the salt from the original salt basin has been expelled seaward beyond the full graben basement low and is found to form a large salt nappe atop this seaward basement high as sediment is found to climb seaward sediments. The salt canopy is thinner at this stage as increased deposition of sediment on top of the canopy is squeezing the salt out, depositing it further seaward. The third keystone graben (KG3) is much larger than it was at 100 hours (30 Ma), growing as it accommodates the continued extension associated with the seaward expulsion of salt from the underlying canopy.

By 180 hours (54 Ma) sedimentation had almost reached the seaward limit of the original salt basin. The canopy was further squeezed by the overlying sediments, forming a weld as the salt formally composing the canopy was expelled seaward. Keystone graben KG3 has been shut down by this stage. A new diapir (D5) has formed just past the seaward limit of the salt basin and is accompanied by an expulsion rollover (ER4) and a keystone graben (KG4). ER4 formed to accommodate the seaward movement of the underlying salt as it was squeezed out of the salt basin onto the seaward basement and into diapir D5. Keystone graben KG4 formed to accommodate the extension associated with the bending of strata in expulsion rollover ER4.

Appendix B - Thermal and Petroleum Systems Modelling Procedures

B-1: About PetroMod 10

PetroMod 10, made by Integrated Exploration Systems in Aachen, Germany, is a basin modelling software package that mathematically simulates the geologic history of a sedimentary basin based on various input data. The input information for this project include 2D seismic interpretations, well data, geological data, and geochemical data. The simulation is based on three primary calculations: heat-flow (to account for the increase in temperature with burial of source and reservoir rocks), the Arrhenius equation (to describe the cracking of kerogen with increasing temperature), and Darcy's law (to deal with the migration of hydrocarbons from source to reservoir) (Wielens et al., 2006).

B-2: 1D modelling procedures

1D models were created for three wells to constrain boundary conditions for the 3D models. Wells were also used to constrain ages and formations within the model area as well as the lithological properties of the sedimentary units. 1D models were created for the Shubenacadie H-100 well (Table B.1), the Torbrook H-100 well (Table B.2), and the Acadia K-62 well (Table B.3). Well locations can be seen in Figure 2.1. For each formation, thickness, absolute age of deposition and generalized rock type are specified. Lack of data did not allow for the use of erosional events.

B-2.1: Assigning boundary conditions

Paleo water depth (PWD), sediment water interface temperature (SWIT), and heat-flow (HF) histories are the boundary assignments for the model. Due to the close proximity of the three wells, the boundary assignments were similar and were set the same for each well.

Name	Top	Base	Present Thickness	Eroded Thickness	Deposition Age from	Deposition Age to	Erosion Age from	Erosion Age to	Lithology
	[meter]	[meter]	[meter]	[meter]	[Ma]	[Ma]	[Ma]	[Ma]	
Banquereau Fm	1476.50	2988.39	1511.89		33.90	0.00			SHALEsand
Top Eocene (Still Banquer	2988.39	3703.00	714.61		75.00	33.90			SHALEcarb
Wyandot Chalk (~Top Cret)	3703.00	3795.00	92.00		85.00	75.00			CHALK
Dawson Canyon Fm	3795.00	4000.00	205.00		95.00	85.00			SHALE
Shortland Shale (Top E. Cr	4000.00	4200.00	200.00		125.00	99.60			SHALE

Table B.1: *Shubenacadie H-100 well data*

Name	Top	Base	Present Thickness	Eroded Thickness	Deposition Age from	Deposition Age to	Erosion Age from	Erosion Age to	Lithology
	[meter]	[meter]	[meter]	[meter]	[Ma]	[Ma]	[Ma]	[Ma]	
Recent-Mid Pliocene	1674.50	2962.00	1287.50		20.00	0.00			SHALE&SILT
Mid Miocene (Tertiary 33)	2962.00	3260.00	298.00		23.03	20.00			SHALE&SILT
Top Oligocene	3260.00	3488.00	228.00		33.90	23.03			SHALE
Top Eocene	3488.00	3600.00	112.00		35.00	33.90			SHALE

Table B.2: *Torbrook C-15 well data*

Name	Top	Base	Present Thickness	Eroded Thickness	Deposition Age from	Deposition Age to	Erosion Age from	Erosion Age to	Lithology
	[meter]	[meter]	[meter]	[meter]	[Ma]	[Ma]	[Ma]	[Ma]	
Banquereau Fm	1405.89	3132.99	1727.10		75.00	0.00			SHALE&SILT
Wyandot Fm	3132.99	3159.69	26.70		85.00	75.00			CHALK
Dawson Canyon Fm	3159.69	3253.99	94.30		95.00	85.00			SHALE
Petrel (~ shortland shale)	3253.99	3317.59	63.60		130.00	95.00			SHALE
Roseway (top missis	3317.59	3845.59	528.00		145.50	130.00			SILT&LIME
Top Abenaki Fm	3845.59	4625.59	780.00		161.20	145.50			LIMEdolom
Misane member	4625.59	4843.59	218.00		167.70	161.20			SAND&SILT
Scatarie member	4843.59	5489.59	646.00		171.60	167.70			LIMEsandy
Mohican equiv.	5489.59	5826.99	337.40		190.00	171.60			LIMEsandy

Table B.3: *Acadia K-62 well data*

PWD was assumed to be 0 m at the time of rifting ~200 Ma, and shows a gradual increase in depth since, reaching a current depth of ~1400 m (Fig. B.1). Because much of the sedimentary column shows signs of shelf deposition, the large increase to present was

kept close to recent. SWIT was kept relatively constant with a gradual decrease from ~20 ºC at 200 Ma to ~4 ºC at present (Fig. B.1). As little work has been published on PWD and SWIT in the Scotian Basin, these curves were interpreted based on the rift history of the region (Louden, 2002) and personal communication with Hans Wielens.

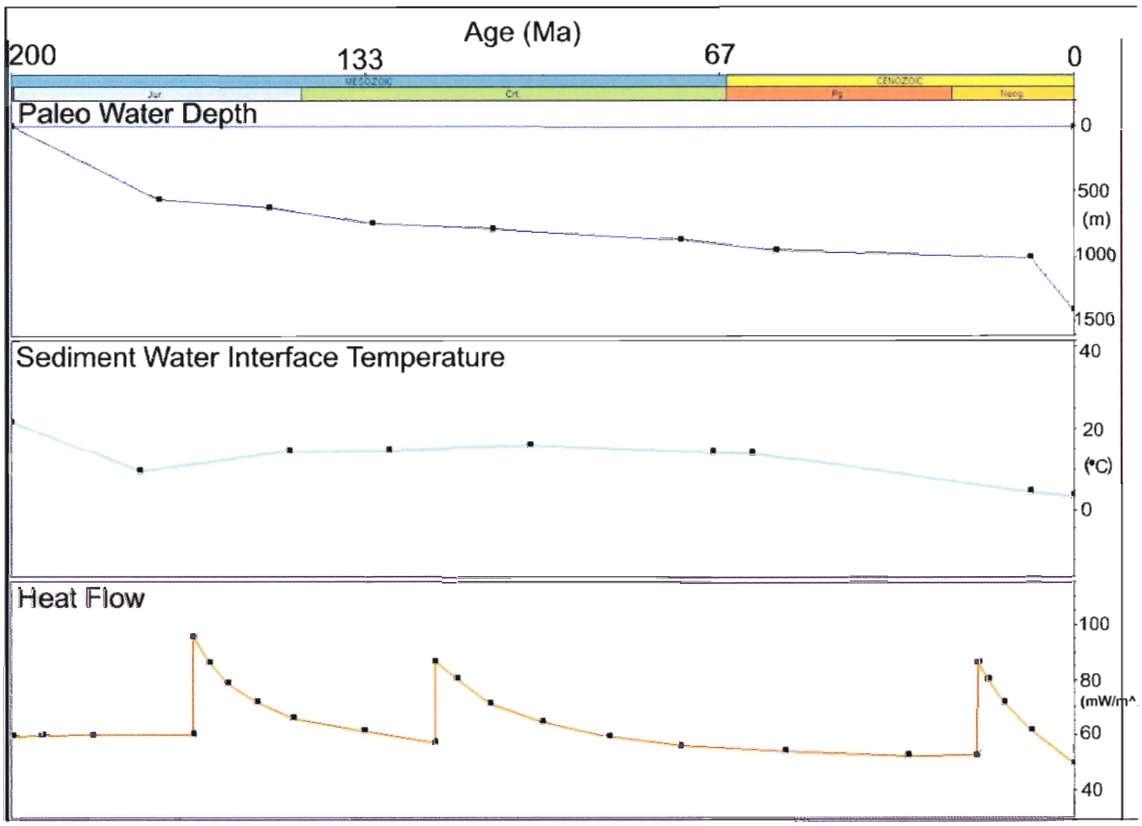

Figure B.1: *Paleo water depth, sediment water interface, and heat-flow curves setting boundary assignments for modelling.*

A basement heat-flow curve was plotted for the entire time span of the model (200 Ma) (Fig. B.1). The curve has a general trend of ~50 mW/m^2. This is significantly higher than the values of 36.5 mW/m^2 predicted by Goutorbe et al. (2007). The higher heat-flow values were needed to concur with the vitrinite reflectance values from the Acadia K-62 well; (Fig. B.2) (Avery, 2004). Three heat spikes can be seen in the HF curve followed by exponential McKenzie decay (McKenzie, 1978). These correspond to the rifting of North America from Africa prior to 160 Ma, the rifting of North America

from Europe at ~120 Ma, and the final heat spike is inferred as a result of the abnormal vitrinite reflectance curve from the Acadia K-62 well.

B-2.2: Vitrinite reflectance data

The vitrinite reflectance data from the Acadia K-62 well (Avery 2004) are characterized by an upper section with abundant kerogen samples, and only one sample at depth (Fig. B.2). The lower sample gave few, poor readings, and thus the slope was weighted to the upper samples (Avery, 2004). The curve is the Ro as calculated by the simulation for the model; changing the heat-flow changes the curve. Thus the best possible fit of the curve is achieved with heat-flow as used in the model. The slope of the line on the graph represents the maturation slope based on the input heat-flow, and in order to have this slope coincide with the measured vitrinite reflectance values, a heat-flow spike within the last 20 Ma is needed (Fig. B.4).

B-3: 2D basin modelling

2D basin modelling was not done as it is used for very precise interpretations of specific features and the goal of this thesis was to determine general trends regarding heat-flow and petroleum systems potential.

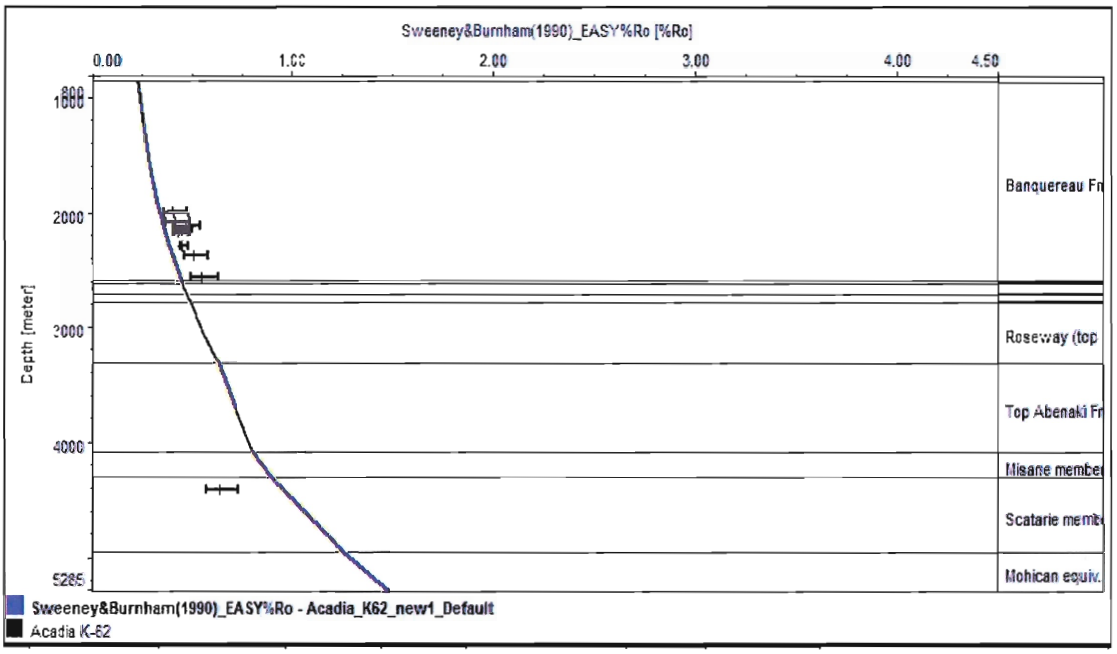

Figure B.2: *Vitrinite reflectance curve, %Ro vs. Depth. %Ro values from Avery (2004)*

B-3.1: Importing surfaces into PetroMod 3D

All horizons picked during seismic interpretations were depth-converted and exported from Kingdom Suite as laterally extensive and continuous surfaces across the entire study area. These files were exported as x,y,z GRD files and later converted to txt files for input into PetroMod. Surfaces were loaded into the Seistrat 3D function of PetroMod in order, from surface to basement. The data points did not all fit the Seistrat grid perfectly and so the surfaces were interpolated between points, using the finite element method to create smooth, continuous surfaces. These interpolations caused the surfaces to be extended well beyond the regions bounded by the seismic lines.

The map stack created in Seistrat 3D was exported as a CPS-3 ASCII format GRD file, which was then loaded into PetroMod 3D for thermal and petroleum systems modelling. Only the base salt was imported into PetroMod 3d as the diapiric structures

caused significant distortions to the surrounding surfaces. The salt diapirs were added later, using the program's "piercing" tool, which not only prevented distortions in the model but also allowed for the timing of diapir growth to be constrained.

B-3.2 Defining the area of interest

As the surfaces were extended beyond the study area outlined in Figure 2.1 during smoothing, an area of interest had to be defined for 3D modelling to restrain the model to initial study area. The study area in the 4D model has been extended ~5 km beyond the edges of the original study area to accommodate for the round 3D shape of salt diapirs interpreted on the seismic lines (Fig. B.3).

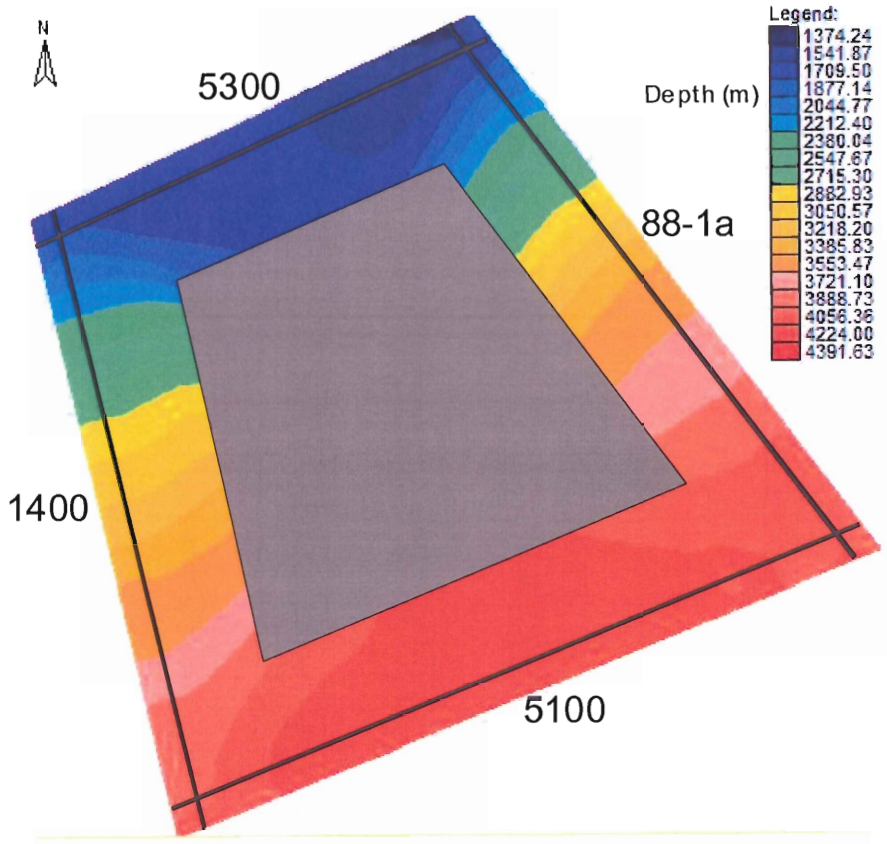

Figure B.3: *Area of interest showing location of seismic lines in black. Base map shows depth to sea floor. Central section is blocked out as smoothing of surfaces causes false topography.*

B-3.3 Correcting for cross cutting layers

A result of extrapolating 2D horizons into 3D surfaces is that some layers may be crossed by others. To correct for this, preference has been given to the overlying layer as with greater depth come greater uncertainties in interpretation as the quality of seismic imaging degrades with depth. When an underlying layer is found crossing an overlying layer it results in incorrect negative thickness values in the thickness table. Changing the underlying thickness value from a negative to a zero gives the unit a thickness of zero, and preference to the overlying layer (Fig. B.4).

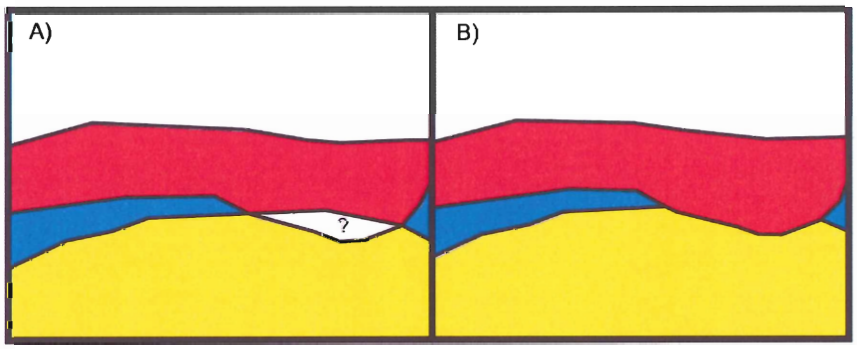

Figure B.4: *In case of overlapping layers precedence is given to top layer. A) before correction, B) after correction.*

B-3.4 Splitting layers

The unit underlying the Wyandot surface contains both the Wyandot chalk and the Dawson Canyon Formation-equivalent shales and silts. Because no mappable reflectors in the seismic images were found that correspond to the Dawson Canyon Formation, the unit underlying this surface was split into two layers, to include the Dawson Canyon Formation in the model. The unit split ranged in thickness from ~100-1500m, and was split giving the upper layer (the Wyandot chalk) 10% of the original

thickness, and the lower layer (the Dawson Canyon equivalents) the remaining 90%. The Missisauga Formation was also split in order to include the potential source rocks of the Verrill Canyon Formation. The Missisauga Formation was split, defining the bottom 20% of the original layer as the Verrill Canyon Formation, and leaving the upper 80% as the Missisauga Formation.

B-3.5 Assigning ages, lithologies and facies

Every layer of the model must be assigned specific ages of deposition, lithologies, and facies. As the picks made in Kingdom represent formation tops, the surfaces imported into PetroMod must also represent the tops of formations. The units between the surfaces are thus assigned the facies/lithologies associated with that formation top. In total 14 layers are present. The formations associated with each surface, their ages of deposition, and variations in facies/lithologies throughout the layers are listed in Table B-4. All facies included in the model and their associated lithologies are listed in Table B.5. Also included in this table are petroleum systems elements and associated rock properties.

Name	Deposition Age from [Ma]	Deposition Age to [Ma]	Erosion Age from [Ma]	Erosion Age to [Ma]	Max. Time Step Duration [Ma]	Facies 1	Facies 2	Facies 3
Banquereau_1_1st	3.60	0.00	0.00	0.00	10.00	Banquereau_1	--	--
Banquereau_2_1132	23.03	3.60	0.00	0.00	10.00	Banquereau_2	--	--
Banquereau_3_1145	33.90	23.03	0.00	0.00	10.00	Banquereau_3	--	--
Banquereau_4_1212	55.00	33.90	0.00	0.00	10.00	Banquereau_4	--	--
Banquereau_5_1224	75.00	55.00	0.00	0.00	10.00	Banq_5_source	Banquereau_5	Banq5_peirced
Wyandot_2111t	85.00	75.00	0.00	0.00	10.00	Wyandot	Wyandot_peirced	--
Dawson_Canyon	95.00	85.00	0.00	0.00	10.00	Dawson_Canyon	Dawson_Canyon_pierced	--
Logan_Canyon_2116	130.00	95.00	0.00	0.00	10.00	Logan_Canyon_reservoir	Logan_Canyon	Logan_C_pierced
Missisauga	142.40	130.00	0.00	0.00	10.00	Missisauga_reservoir	Missisauga	Miss_pierced
Verrill_Canyon	145.50	142.40	0.00	0.00	10.00	Verrill Canyon	Verrill_Canyon_pierced	--
Baccaro_2212	161.20	145.50	0.00	0.00	10.00	Baccaro	Baccaro_pierced	--
Misane_2213	167.70	161.20	0.00	0.00	10.00	Misane	Misane_pierced	--
Scatarie_2222	190.00	167.70	0.00	0.00	10.00	Scatarie	Scatarie_pierced	--
Argo_Salt	200.00	190.00	0.00	0.00	10.00	Scatarie	Argo_Salt	--
Basement	210.00	200.00	0.00	0.00	10.00	basement	--	--

Table B.4: *Layers in model named after their corresponding formations. Also shows associated ages of deposition, and facies within each layer.*

Name	Petroleum System Elements	Color	Lithology Value	TOC Model	TOC Value [%]	Kinetics	HI Value [mgHC/gTOC]
Banquereau_1	none		SHALE&SILT	Uniform	0.00	none	0.00
Banquereau_2	none		SHALE&SILT	Uniform	0.00	none	0.00
Banquereau_3	none		SHALE&SILT	Uniform	0.00	none	0.00
Banquereau_4	none		SHALE&SILT	Uniform	0.00	none	0.00
Banq_5_source	Source Rock		SHALE	Uniform	5.00	Pepper&Corvi(1995)_TII(B)	500.00
Banquereau_5	none		SHALE&SILT	Uniform	0.00	none	0.00
Wyandot	none		CHALK	Uniform	0.00	none	0.00
Dawson_Canyon	none		SHALE&SILT	Uniform	0.00	none	0.00
Logan_Canyon_reservoir	Reservoir Rock		SHALE&SAND	Uniform	0.00	none	0.00
Logan_Canyon	none		SHALE&SAND	Uniform	0.00	none	0.00
Mississauga_reservoir	Reservoir Rock		SANDSTONE	Uniform	0.00	none	0.00
Mississauga	none		SHALE&SILT	Uniform	0.00	none	0.00
Baccaro	none		SHALE&LIME	Uniform	0.00	none	0.00
Misane_source	Source Rock		SHALE	Uniform	5.00	Pepper&Corvi(1995)_TII(B)	500.00
Misane	none		SHALE	Uniform	0.00	none	0.00
Scatarie	none		LIMESTONE	Uniform	0.00	none	0.00
Argo_Salt	none		SALT	Uniform	0.00	none	0.00
basement	none		BASEMENT	Uniform	0.00	none	0.00
Wyandot_peirced	none		SALT	Uniform	0.00	none	0.00
Dawson_Canyon_pierced	none		SALT	Uniform	0.00	none	0.00
Logan_C_pierced	none		SALT	Uniform	0.00	none	0.00
Miss_pierced	none		SALT	Uniform	0.00	none	0.00
Baccaro_pierced	none		SALT	Uniform	0.00	none	0.00
Misane_pierced	none		SALT	Uniform	0.00	none	0.00
Scatarie_pierced	none		SALT	Uniform	0.00	none	0.00
Banq5_peirced	none		SALT	Uniform	0.00	none	0.00

Table B.5: *Table showing all assigned facies, associated colour, petroleum systems elements and properties.*

B-3.6 Putting in salt diapirs

Salt diapirs were entered once all layers were assigned primary lithologies, ages, and facies. As analogue model Experiment 5-7 shows, salt diapirs pierce the surface and grow simultaneously with sedimentation and thus the ages of the piercing diapirs were interpreted to be equal in age as the layers they pierced. The outlines of diapirs were

Geological Facies	Piercing Time [Ma]	Piercing Lithology
Wyandot_pierced	85.00	SALT
Logan_C_pierced	130.00	SALT
Baccaro_pierced	161.20	SALT
Misane_pierced	167.70	SALT
Scatarie_pierced	190.00	SALT
Dawson_Canyon_pierced	95.00	SALT
Verrill_Canyon_pierced	145.50	SALT
Banq5_peirced	75.00	SALT
Miss_pierced	142.40	SALT

Table B.6: *Salt piercing table showing age at which salt pierced layers*

drawn on the facies surface map of each layer and the age at which the diapirs pierced each layer was specified in the piercing table (Table B.6). Locations of salt diapirs were inferred from seismic interpretations of lines 88-1a and 1400 (Fig.'s 2.2 and 2.3), and they given rounded shapes in surface view. The lithology within the region specified by the piercing diapirs was then changed to salt for each layer, and the facies within the pierced region was changed to "facies_pierced".

B-3.7 Running the simulator

Once all required input information was set, a simulation was run to calculate the 4D heat-flow, geothermal gradient, and petroleum systems resulting from the input parameters. Two simulations were run, one for model 1 with the Misane source rock and one for model 2 with the Verrill Canyon source rock.